General Disclaimer

One or more of the Following Statements may affect this Document

- This document has been reproduced from the best copy furnished by the organizational source. It is being released in the interest of making available as much information as possible.

- This document may contain data, which exceeds the sheet parameters. It was furnished in this condition by the organizational source and is the best copy available.

- This document may contain tone-on-tone or color graphs, charts and/or pictures, which have been reproduced in black and white.

- This document is paginated as submitted by the original source.

- Portions of this document are not fully legible due to the historical nature of some of the material. However, it is the best reproduction available from the original submission.

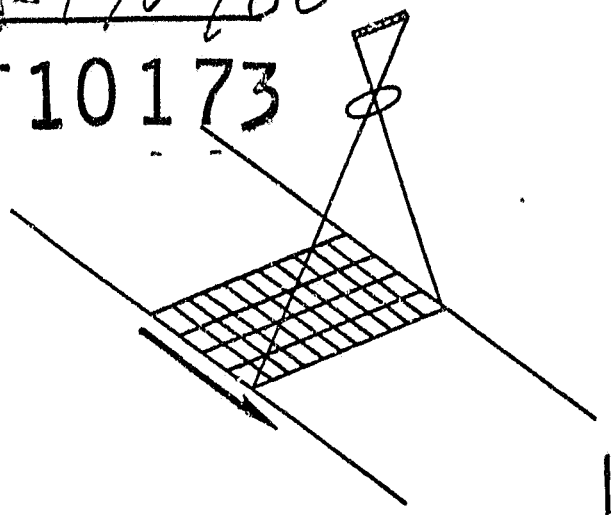

MRS "PROOF-OF-CONCEPT" STUDY ON ATMOSPHERIC CORRECTIONS

ATMOSPHERIC CORRECTIONS USING AN ORBITAL, POINTABLE IMAGING SYSTEM

By
Dr. Philip N. Slater

January 1980

PREPARED FOR
NASA—
GODDARD SPACE FLIGHT CENTER
GREENBELT, MD. 20771

BY
ORI, INC.
1400 SPRING ST.
SILVER SPRING, MD 20910

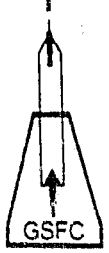

UNCLASSIFIED

SECURITY CLASSIFICATION OF THIS PAGE (When Data Entered)

REPORT DOCUMENTATION PAGE		READ INSTRUCTIONS BEFORE COMPLETING FORM
1. REPORT NUMBER TR 1653	2. GOVT ACCESSION NO.	3. RECIPIENT'S CATALOG NUMBER
4. TITLE (and Subtitle) MRS 'PROOF-OF-CONCEPT' ON ATMOSPHERIC CORRECTIONS ATMOSPHERIC CORRECTIONS USING AN ORBITAL POINTABLE IMAGING SYSTEM		5. TYPE OF REPORT & PERIOD COVERED FINAL 5/15/79-1/15/80 6. PERFORMING ORG. REPORT NUMBER
7. AUTHOR(s) Dr. Philip N. Slater		8. CONTRACT OR GRANT NUMBER(s) NAS5-25606
9. PERFORMING ORGANIZATION NAME AND ADDRESS ORI, Inc. 1400 Spring St. Silver Spring, MD 20910		10. PROGRAM ELEMENT, PROJECT, TASK AREA & WORK UNIT NUMBERS
11. CONTROLLING OFFICE NAME AND ADDRESS NASA/GSFC Code 942 Greenbelt, MD 20771		12. REPORT DATE January, 1980 13. NUMBER OF PAGES
14. MONITORING AGENCY NAME & ADDRESS (if different from Controlling Office) ORI, Inc. 1400 Spring St. Silver Spring, MD 20771		15. SECURITY CLASS. (of this report) UNCLASSIFIED 15a. DECLASSIFICATION/DOWNGRADING SCHEDULE

16. DISTRIBUTION STATEMENT (of this Report)

25 copies to Dr. Charles Schnetzler
Code 942
NASA-GSFC
Greenbelt, MD 20771

17. DISTRIBUTION STATEMENT (of the abstract entered in Block 20, if different from Report)

18. SUPPLEMENTARY NOTES

. Slater of the University of Arizona is a consultant to ORI, Inc.

19. KEY WORDS (Continue on reverse side if necessary and identify by block number)

OPTICAL THICKNESS	SCIENCE CLASSIFICATION	TRANSMITTANCE
RADIATIVE TRANSFER	HAZE	AEROSOL
MULTISPECTRAL	SPECTRAL SIGNATURE	PATH RADIANCE
REMOTE SENSING	SATELLITE SIMULATION	

20. ABSTRACT (Continue on reverse side if necessary and identify by block number)

This report describes a preliminary study of the feasibility of using a pointable imager to determine atmospheric parameters. In particular the study was directed toward simulating the determination of the atmospheric extinction coefficient and the path radiance, the two quantities that have to be known in order to correct spectral signatures for atmospheric effects.

The study included the consideration of the geometry of ground irradiance and observation conditions for a pointable imager in a Landsat orbit as a

DD FORM 1 JAN 73 1473 EDITION OF 1 NOV 65 IS OBSOLETE
S/N 0102-014-6601

UNCLASSIFIED

SECURITY CLASSIFICATION OF THIS PAGE (When Data Entered)

function of time of year. A simulation study was conducted on the sensitivity of scene classification accuracy to changes in atmospheric condition. A two-wavelength and a non-linear regression method for determining the required atmospheric parameters were investigated.

The results of this preliminary study are promising and indicate the feasibility of using a pointable imaging system (a) for the determination of the atmospheric parameters required to improve classification accuracies in urban-rural transition zones and to apply in studies of BRDF and polarization effects and (b) for the determination of the spectral reflectances of ground features.

FOREWORD

The Multispectral Resource Sampler (MRS) "Proof-of-Concept" Study is intended to be a comprehensive analysis of the corrections that must be applied to MRS data to allow for atmospheric correction factors and the variability of bidirectional reflectance from the scene.

This study was initiated by Dr. Charles Schnetzler of NASA Goddard Space Flight Center, and was performed by ORI, Inc. Space Data and Systems Division with Mr. Charles W. Aitken coordinating the efforts of ORI's consultants.

The complete study results are reported in five separate volumes which have the following titles and authors:

DETERMINATION OF ATMOSPHERIC OPTICAL PARAMETERS USING THE MULTISPECTRAL RESOURCE SAMPLER, by Dr. Robert E. Turner, Science Applications, Inc.

ATMOSPHERIC CORRECTION USING AN ORBITAL POINTABLE IMAGING SYSTEM By Dr. Philip N. Slater, University of Arizona

A SIMULATION ANALYSIS OF BIDIRECTIONAL REFLECTANCE PROPERTIES AND THEIR EFFECTS ON SCENE RADIANCE--IMPLICATIONS FOR THE MRS, By Dr. James A. Smith, Colorado State University

MRS LITERATURE SURVEY OF BIDIRECTIONAL REFLECTANCE, By Dr. James A. Smith, Colorado State University

MRS LITERATURE SURVEY OF ATMOSPHERIC CORRECTIONS By, Dr. Philip N. Slater, University of Arizona

ORI, Inc. would like to acknowledge the invaluable assistance of the following people who helped in the performance of this study:

Dr. P.N. Slater (Principal Investigator Atmospheric Corrections)	University of Arizona
Gen. R.S. Browning	University of Arizona
Dr. B. M. Herman	University of Arizona
Mr. S. J. Martinek	University of Arizona
Dr. R.A. Schowengerdt	University of Arizona
Dr. J. A. Smith (Principal Investigator Bidirectional Reflectance)	Colorado State University
Mr. K. J. Ranson	Colorado State University
Ms. J. A. Kirchner	Colorado State University
Dr. R. E. Turner (Principal Investigator Atmospheric Corrections)	Science Applications, Inc.

ORI
Silver Spring, Maryland 20910

ATMOSPHERIC CORRECTIONS USING AN ORBITAL POINTABLE IMAGING SYSTEM

PREPARED BY:

DR. PHILIP N. SLATER
UNIVERSITY OF ARIZONA

CONSULTANT TO:

ORI, INC.
SILVER SPRING, MARYLAND

LIST OF CONTRIBUTORS

This report includes contributions from the following:

R. S. Browning	(provided data from atmospheric radiative transfer model)
B. M. Herman	(consulted on atmospheric considerations)
S. J. Martinek	(developed the non-linear regression method)
R. A. Schowengerdt	(worked on the effect of the atmosphere on classification accuracy)
P. N. Slater	(principal investigator)

TABLE OF CONTENTS

1.0 INTRODUCTION

Methods for the correction of Landsat data for astmopheric transmittance and path radiance have thus far relied on the use of atmospheric models and/or extensive ground-based measurements. The use of an orbiting pointable imager may allow atmospheric corrections to be made without any supporting ground measurements or any knowledge of the ground reflectance. If a pointable imager were launched with the Thematic Mapper (TM) and/or the Multispectral Scanner System (MSS), or if it were flown in close orbital proximity to such sensors, then it might be possible to correct the data, collected by these systems for atmospheric effects for any area of the earth's surface.

The following preliminary study was conducted to consider the feasibility of such a correction method because of its potential importance in improving scene classification accuracy, correcting bi-directional reflectance distribution function (BRDF) data, correcting obligue angle data collected for biomass estimation in sparsely vegetated areas, and for use in the analysis of the results of polarization experiments.

1.1 PROJECT OUTLINE

The work performed as part of this project has included:

1) A literature survey of work in determing the influence of atmospheric effects on spectal signatures and classification accuracies. Over sixty references were listed and six chat were particularly relevant to classification accuracy were discussed in detail. This survey was described in a report entitled "MRS Literature Survey of Atmospheric Corrections". (MRS is an abbreviation for Multispectral Resource Sampler).
2) The spherical geometry of earth sensing from a pointable sensor in a Landsat orbit was examined. This is of value for work in both bi-directional reflectance distribution function (BRDF) studies as well as atmospheric correction. The ranges of solar aximuthal zenith angles, and Air mass which can be encountered as a function of latitude and time of year are described as a function of pointing angle.
3) The literature survey, mentioned in item (1) above, revealed that changes in atmospheric extinction coeffecient (or optical thickness), τ_{ext}, greater than 0.1, between training and test site, began to have a significant effect on classification accuracy. A study is reported here that was made to corroborate this result and determine the sensitivity of classification accuracy to change in atmospheric effects.
4) A two-wavelength, single target method for determining τ was investigated in detail but was found to underestimate τ_{ext} because the rate of change in path radiance (L_p) with pointing angle, θ , was greater than the rate of change in total radiance (L_s) at the sensor.
5) A non-linear regression method is described which enables τ_{ext}, path radiance, Lp, the reflectance, ρ, of a uniform Lambertian ground feature to be determined from a knowledge of the variation of the radiance at the sensor, L_s, with pointing angle θ, for a particular wavelength interval $\Delta\lambda$.

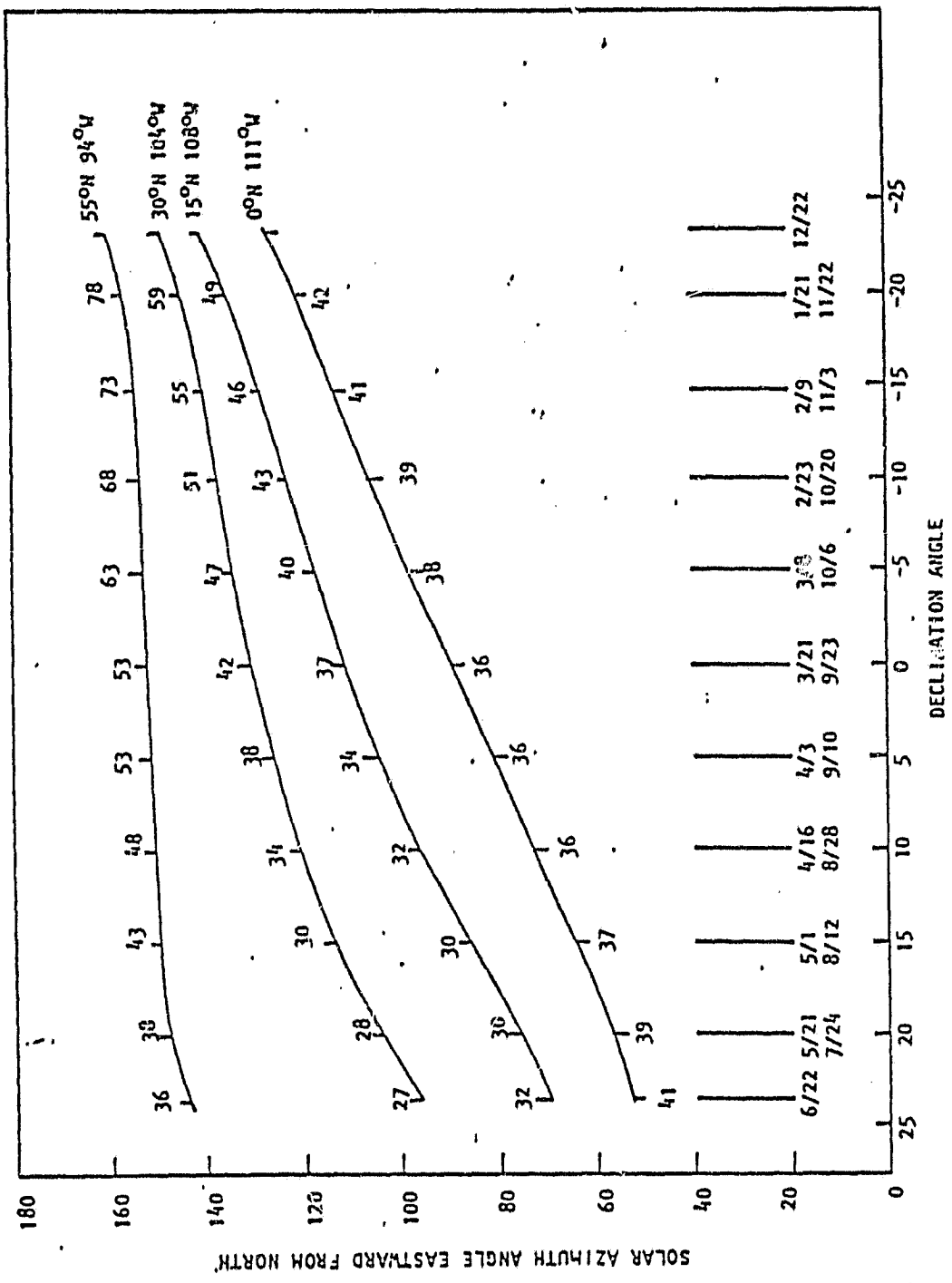

Figure 1. Plot of solar azimuth angle versus solar declination angle for a typical Landsat orbit (see text). The day and month of the year and the solar zenith angle are marked for 5° increments of declination angle. The latitudes considered are 0°, 15°N, 30°N and 55°N.

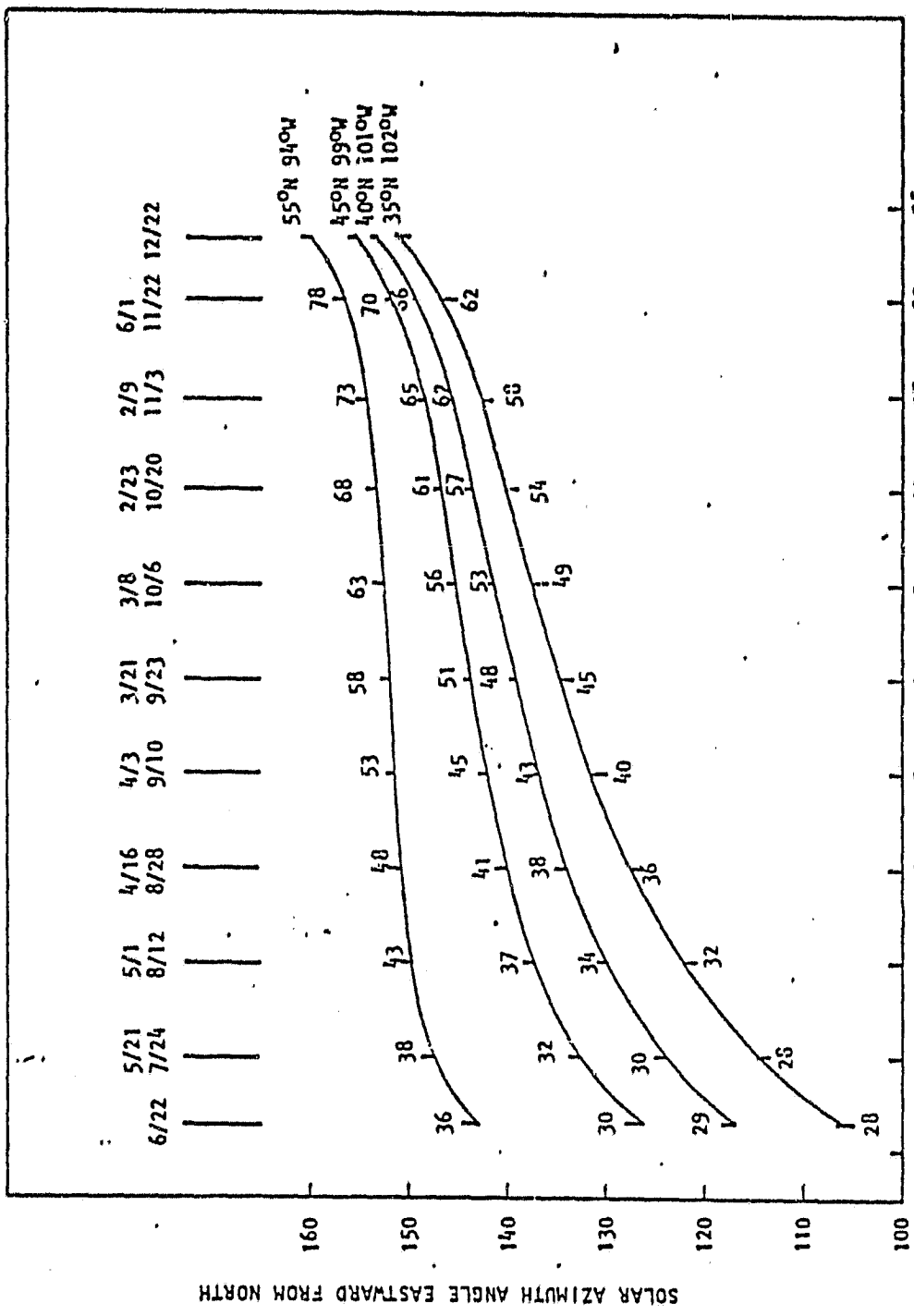

Figure 2. Plot of solar azimuth angle versus solar declination angle for a typical Landsat orbit. The day and month of the year and the solar zenith angle are marked for 5° increments of declination angle. The latitudes considered are 35°N, 40°N, 45°N and 55°N.

The size of the Instantaneous Field of View (IFOV) projected on to the ground as a function of pointing angle is important because it indicates the size of the uniform ground reference area required for accurate atmospheric and BRDF measurements. Figure 3 shows the increase in size of an IFOV 15 m X 15 m at the ground at nadir as the pointing angle to nadir increases. The case considered is that for an orbital altitude of 700 km and the effect of earth curvature has been taken into account. It is worth noting for comparison purposes that the IFOV length equals that of the MSS IFOV (76 m) at an angle of about 56^{o}. The pointing direction becomes tangential to the earth's surface at a pointing angle to nadir of about 66^{o}.

The position of the sensor in its orbit with respect to a reference area on the ground for various pointing angles is shown in Figure 4. Again the orbital altitude is 700 km. The adjacent table indicates that a maximum air mass of 4 is encountered where the pointing angle is nearly tangential to the earth's surface, at 65^{o}, in orbital position E.

The general atmospheric problem in remote sensing is illustrated in Figure 5. The figure shows radiant flux from the sun incident on two ground areas B and A and a remote sensing system pointed at area B. As the direct flux from the sun passes through the atmosphere to the ground it is attenuated by scattering and absorption. (We shall assume here that we are sensing through non-absorbing spectral regions of the atmosphere.) The ground area B is irradiated primarily by direct solar flux partially attenuated by scattering such as indicated at C. In addition there is a diffuse component of the irradiance due to scattering in the atmosphere shown schematically as originating from G but actually coming from the entire hemisphere over the ground area. Flux reflected from B is attenuated by scattering, such as at F, on its path from the ground to the remote sensing system. In addition scattered direct solar flux, as at D, is directed into the entrance pupil of the sensor. There is also a crosstalk component owing to flux reflected from area A being scattered in the direction into the sensor entrance pupil as at E. These last two scattered flux components are indistinguishable from the flux coming from the surface of interest and are commonly referred to as path radiance. (Owing to multiple scattering effects in the atmosphere there are other components of path radiance, however the two shown in Figure 5 are in general the largest contributors). A point worth noting with respect to Figure 5 is that the magnitude of the components contributing

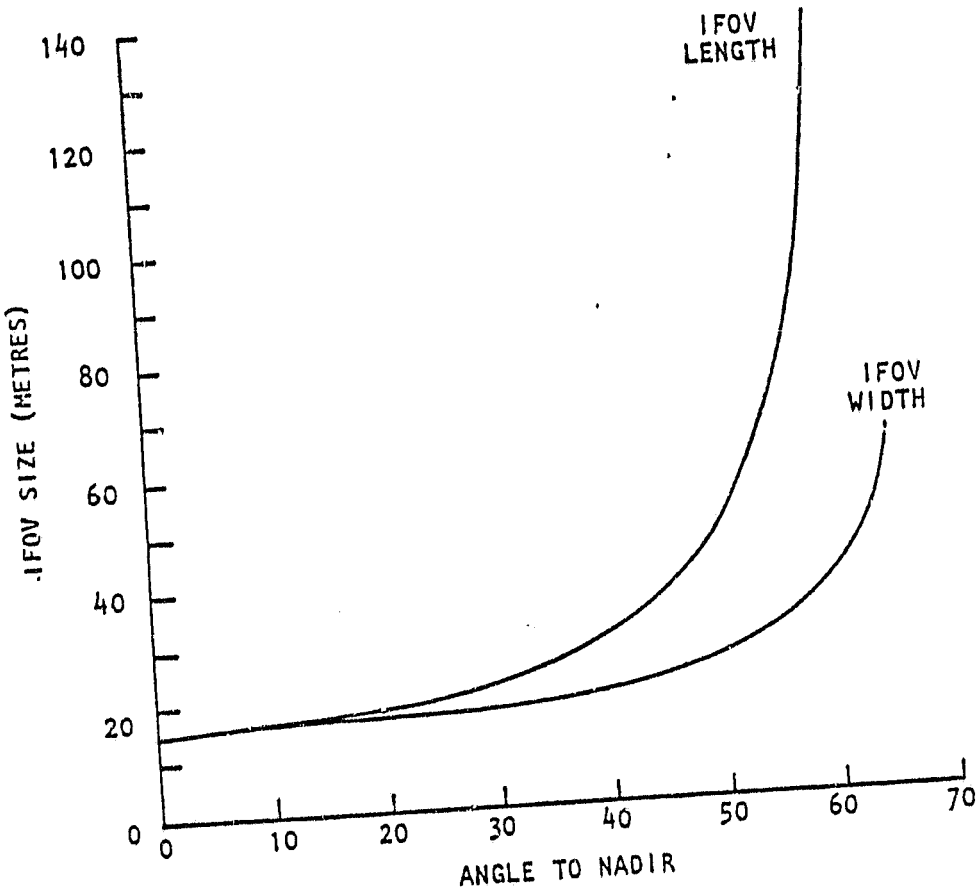

Figure 3. A plot of the ground-projected IFOV dimensions for a sensor, at an altitude of 700 km, having a 15m x 15m nadir IFOV.

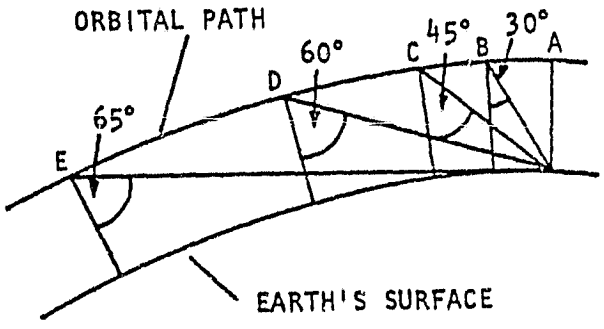

ORBITAL POSITION OF SENSOR	ANGLE OFF NADIR, θ_N	AIR MASS
A	0°	1.0
B	30°	1.14
C	45°	1.5
D	60°	2.4
E	65°	4.0

A

Figure 4. A diagram showing the position of a pointable sensor with respect to a fixed ground scene as a function of pointing angle. The adjacent table shows the increase of air mass with increase in pointing angle, (Slates, 1980).

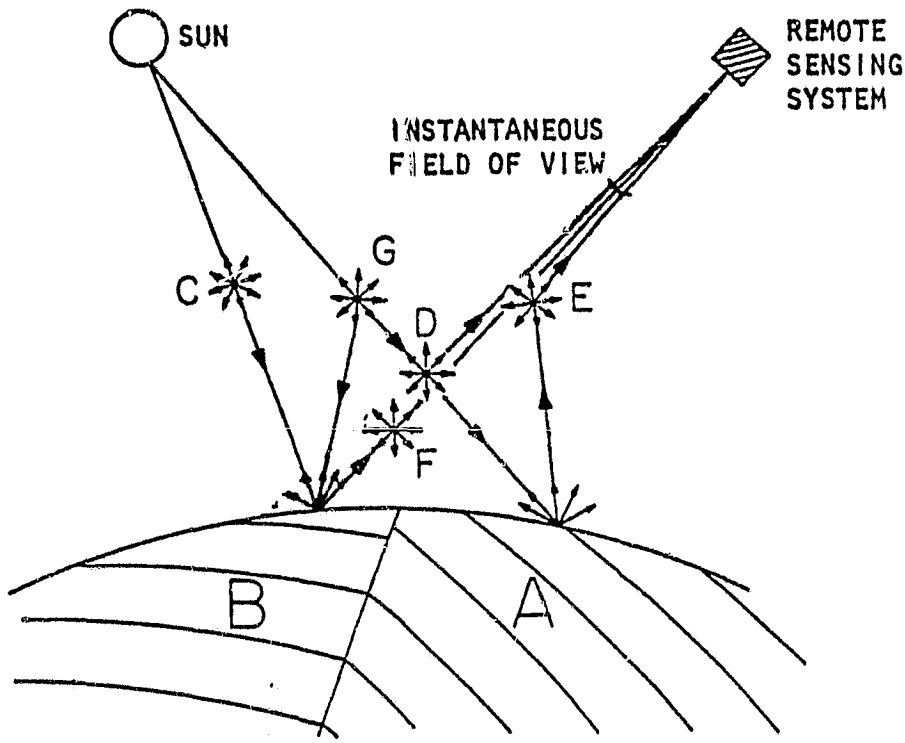

Figure 5. Illustration of the main atmospheric scattering sources contributing to the irradiance at the ground and the total radiance level at the entrance pupil of the sensor, (see text) (Slates, 1980).

to path radiance change with pointing angle. For example, as the pointing angle is increased from nadir to near-tangential, the radiance of the ground surrounding the reference area will provide an increased contribution to the path radiance.

The desirability of a large change in air mass between the ground and sensor in order to have a large variation in sensor radiance to measure is tempered by the above considerations as well as a number of engineering factors. These are summarized below:

1. If horizontal inhomogenieties in atmospheric conditions exist in the region of the reference area, the interpretation of the sensed data will become more difficult as the pointing angle increases.
2. The greater the pointing angle, the larger the ground-projected IFOV and the larger the uniform ground reference area has to be.
3. The influence of the radiance of the surround on the total radiance at the sensor increases with increase in pointing angle. This "crosstalk" effect will complicate the interpreation of the data and reduce the accuracy of the measurement results.
4. Large pointing angles require a larger and heavier pointing mirror with a greater moment of inertia than otherwise necessary.
5. The larger the continuous pointing angle sweep made per target, the fewer the number of observations possible. Reference to Figure 6 shows that a sweep in pointing angle from 63^{0} to 0^{0} takes about 300s, which is about the time for the spacecraft to cross the forty-eight states. In otherwords, if such a large continuous angular sweep is required, no other near-nadir observations could be made of the United States during that particular orbital pass. In comparison, a 45^{0} pointing angle sweep takes 100s.

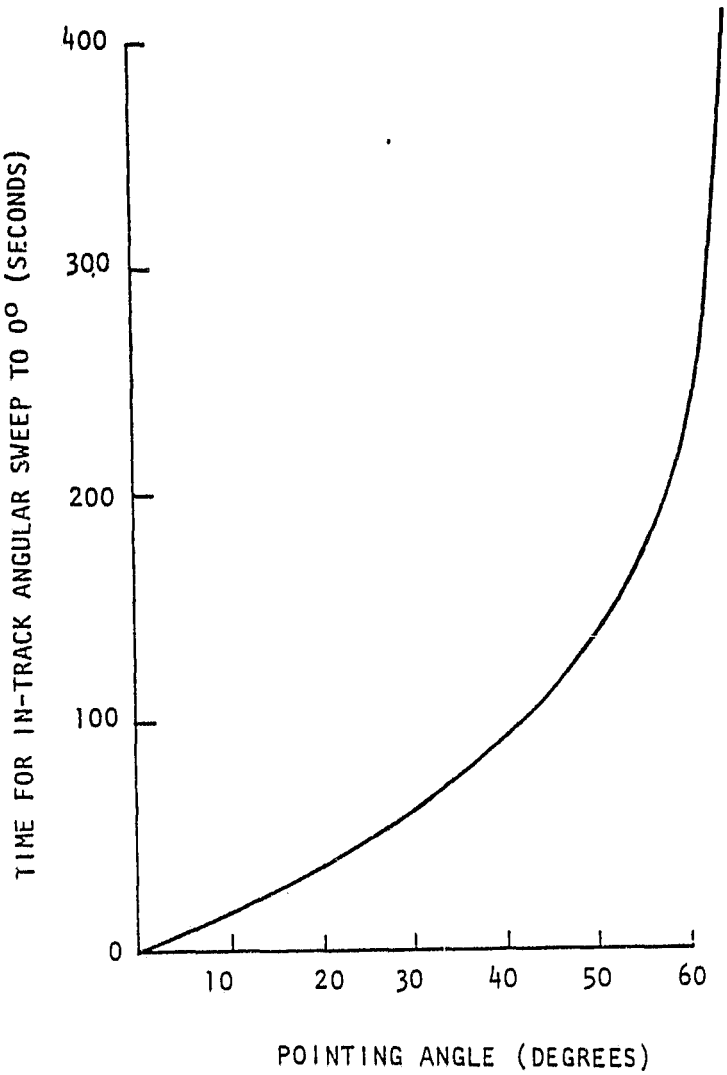

Figure 6. The relation between continuous in-track angular sweep time and pointing angle.

3.0 SENSITIVITY OF CLASSIFICATION ACCURACY TO ATMOSPHERIC CHANGES

A conclusion from the literature survey conducted at the start of this project and reported in "MRS Literature Survey of Atmospheric Corrections" was that changes in the atmospheric extinction coefficient τ_{ext} greater than 0.1 caused a substantial decrease in classification accuracy. The work described in this section was carried out to independently verify these earlier results using a different approach and to develop a more complete understanding of the relationship between changes in τ_{ext} and scene classification accuracy.

To gain an appreciation for the magnitude of τ_{ext} at different sites across the US, we refer to the work of Flowers et al. (1969) who determined the cumulative frequencies of the daily average turbidity for typical urban, suburban and rural conditions. Note that the turbidity coefficient, B, used by Flowers et al. is the decadic extinction coefficient at a wavelength of 0.5 μm and is related to the often-used atmospheric extinction coefficient, or optical depth, τ, by $B = 2.3\tau$. τ is often quoted for λ = 0.55 μm whereas Flowers, et al., used B values at 0.5 μm. The effect of the change in wavelength depends on Rayleigh scattering and the atmospheric aerosol distribution; however, as a first approximation $\tau_{0.55} = 0.9\tau_{0.5}$. The plot of Flowers, et al., for sites across the United States, of the cumulative frequencies of the daily average turbidity for typical urban, suburban and rural conditions is presented in tabular form in Table 1 in terms of optical depth τ for a wavelength of 0.5 μm. (The subscript 'ext' has been omitted). Note that 95% of the days in rural areas have τ values of less than 0.3 which corresponds in a standard atmosphere, to a visibility or meteorological range of 25 km.

If only changes in τ of greater than 0.1 across a scene significantly reduce classification accuracy, then the results of Flowers, et al., show that the classification of purely rural areas will usually be independent of atmospheric conditions. However, in other cases, for example in land use studies at urban - rural interfaces, changes in τ across the scene can be expected to be much larger than 0.1. Thus the table of Flowers, et al.,

TABLE 1

PERCENT OF DAYS WITH HAZE LEVEL IN INDICATED RANGE

	Lower/upper bounds for τ				
	0/0.1	0.1/0.2	0.2/0.3	0.3/0.4	0.4/∞
Rural	10	65	20	4	1
Suburban	7	28	35	12	18
Urban	2	13	15	15	55

shows that 65% of the days in a typical rural area have τ values between 0.1 and 0.2 and 55% of the days in a typical urban area have τ values greater than 0.4.

In this study of the influence of the change in atmospheric conditions on classification accuracy and later, in the study of methods to determine atmospheric parameters from measurements made by a pointable imager, atmospheric data were derived from a radiative transfer calculation technique described by Herman and Browning (1975). This technique utilized model atmospheres constructed by Elterman with various amounts of aerosol loading. The model assumed a flat earth, a uniform Lambertian surface and a horizontally homogeneous atmosphere. All orders of multiple scattering were considered in the computations. Polarization data are available from this calculation but were not used in these preliminary investigations. The output from the radiative transfer computation gave the total radiance and path radiance emerging from the top of the atmosphere and the total irradiance at the ground for various viewing azimuth angles and view angles to nadir (pointing angles) as a function of ground reflectance, solar zenith angle, wavelength and atmospheric extinction coefficient.

A range of the atmospheric spectral extinction coefficients used as input to the Herman and Browning model are shown in Fig. 7. A Rayleigh atmosphere is shown as the lowest curve, the next is a very clear atmosphere typical of the desert southwest on a day of greater than 100 km visibility. The next three curves are for τ values at 0.65 μm that increase in steps of 0.05. The top curve is for very poor meteoroligical conditions, a τ value of 0.65 at 0.5 μm. It is unlikely that classification work would be attempted under atmospheric conditions as poor as this.

The remote sensing data used to provide the classification for the generation of simulated data were Landsat MSS Computed Compatible Tape (CCT) values taken from an image of the San Carlos Indian reservation, an arid, rural region in central Arizona. The meteorological conditions were excellent at the time the imagery was collected, corresponding to the curve labeled 'very clear' in Fig. 7. (This is an estimate as no atmospheric measurements were taken at the time the imagery was collected and only qualitative reports of the atmospheric condition are available). Simulated

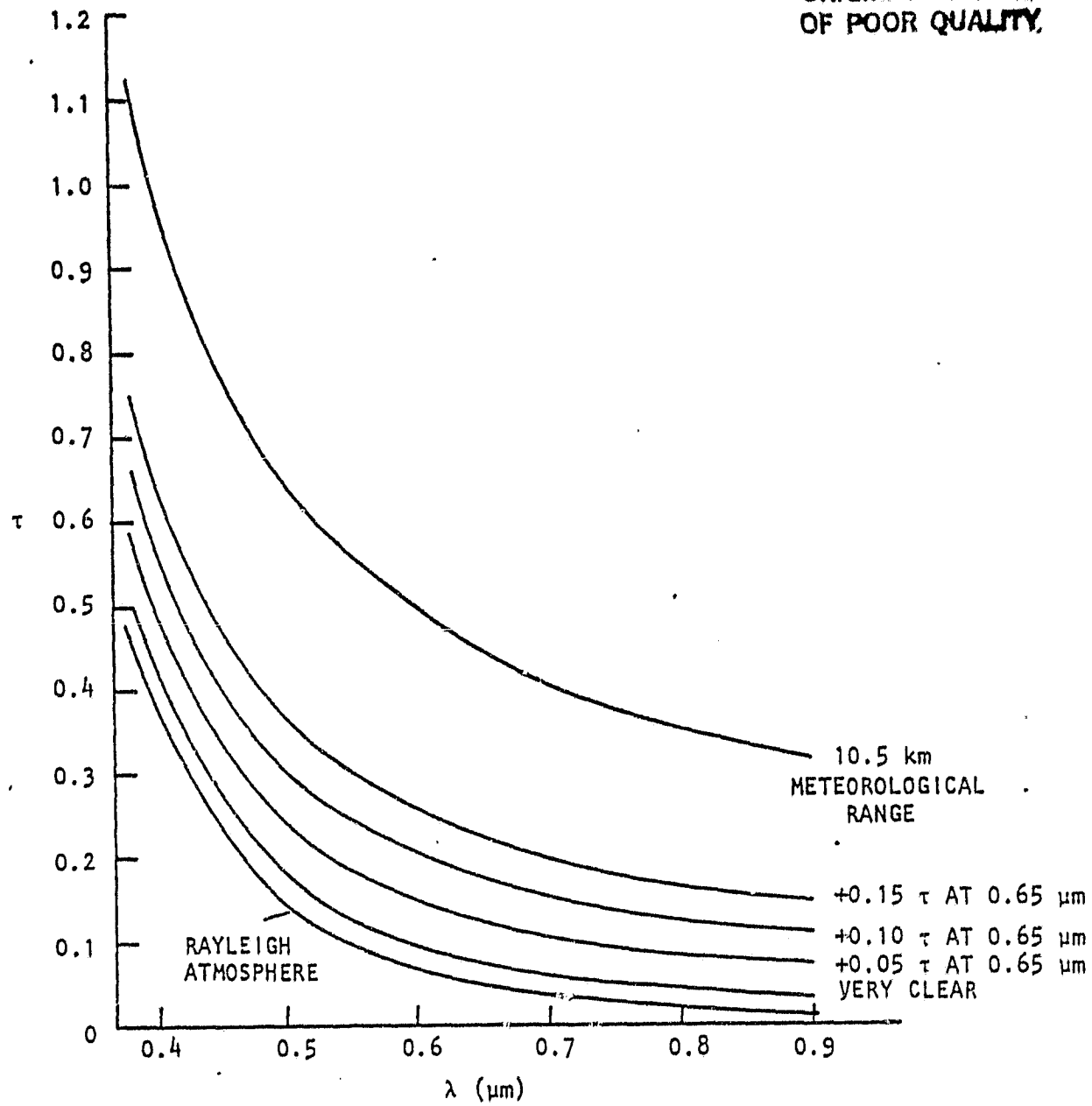

Figure 7. Atmospheric extinction coefficient as a function of wavelength for various atmospheric conditions.

data were generated from the Landsat CCT in four steps:

1. Three surface classes were selected from the imagery: limestone, riparian vegetation and basalt. These were selected because they cover a reasonably comprehensive range of reflectances and spectral characteristics. The riparian vegetation was fairly dense (cover > 60%) but the relatively high reflectance values in bands 4 and 5 are indicative of the influence of underlying soil and rock on the signature. The means and standard deviations of the gray levels for the limestone, vegetation and basalt areas are shown in Fig. 8 for the four MSS bands. (Note that the band 7 values were multiplied by 2 to account for the difference in the quantization range of the data (0 - 63 instead of 0 - 127).
2. The simulated data were first generated as normally distributed independent random numbers with zero mean and unit variance, independently in each of the four spectral bands for each class.
3. Using the eigenvector and eigenvalue matrices and mean vectors of the specified classes, these data were transformed to new data with the desired mean and covariance matrices of the Landsat test classes. Since all the transformations were linear, the final data were also normal independent random variables. Table 2 lists mean, variance, and covariance and correlation matrices for the basalt, limestone and vegetation training classes. Each class consisted of 2400 pixels, quantized to 128 gray levels.
4. Using path radiance values generated from the Herman and Browning atmospheric model, the synthetic image data were transformed from the originally assumed τ value of 0.125 at 0.55 μm to τ values of 0.25 and 0.56. An important point to note here is that the <u>difference between the original and the transformed data is purely deterministic</u>. Thus there is no inclusion of natural deviations between training and test sites. The classification analysis depends only on the different atmospheric conditions assumed.

Fig. 9 is a gray level picture of the synthetic data set for band 4. The top three pictures are for the very clear atmosphere, τ = 0.125, and the bottom three pictures are for the τ = 0.56 case. Note how the contrast

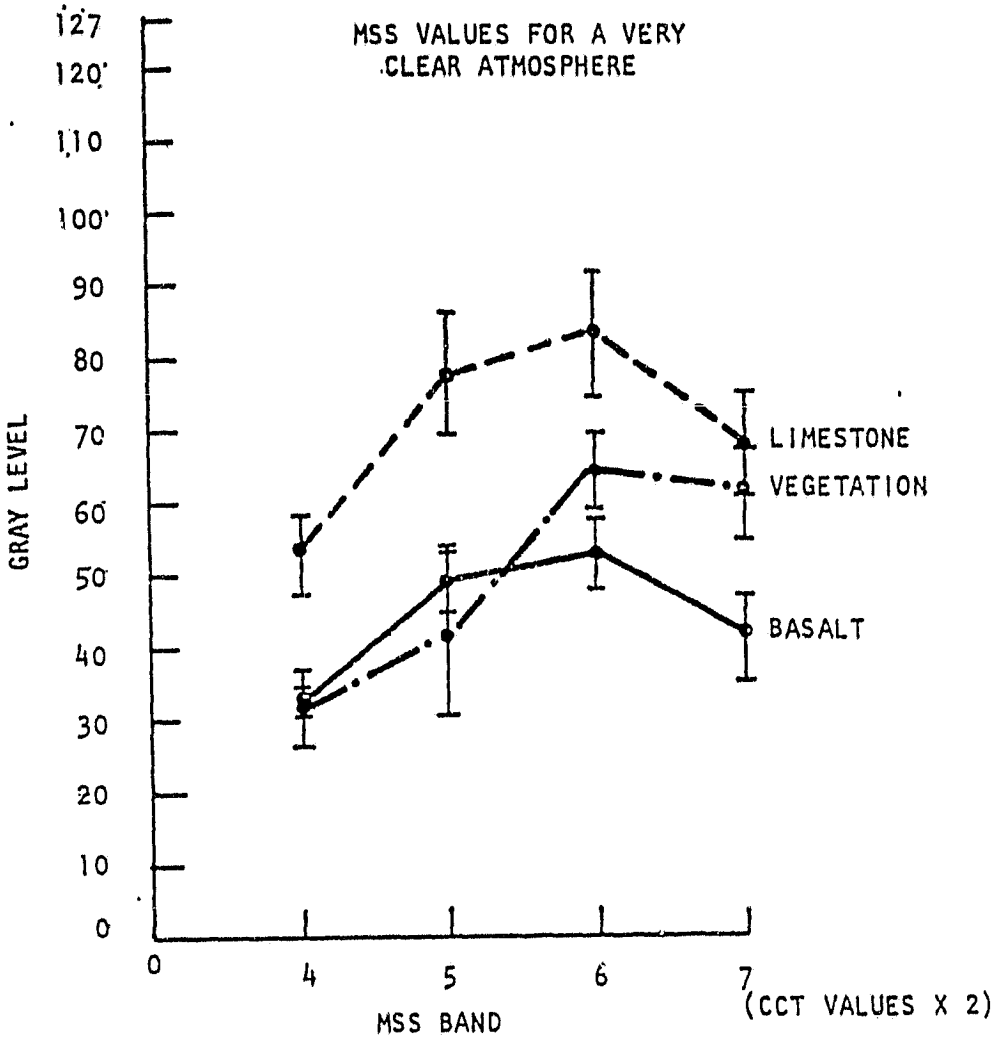

Figure 8. The mean and standard deviation gray levels for limestone, vegetation and basalt as recorded by the four Landsat MSS bands under very clear atmospheric conditions.

TABLE 2

LIMESTONE

THE COVARIANCE AND MEAN FOR TRAINING CLASS LIMESTONE

	500-600	600-700	700-800	800-1100
MEAN	53.12	77.19	82.36	67.05
ST DEV	5.65	8.42	9.06	7.79

COVARIANCE MATRIX

	500-600	600-700	700-800	800-1100
500-600	31.87			
600-700	42.66	70.92		
700-800	42.38	71.61	82.08	
800-1100	34.50	60.90	65.69	60.64

CORRELATION MATRIX

	500-600	600-700	700-800	800-1100
500-600	1.00			
600-700	.90	1.00		
700-800	.83	.94	1.00	
800-1100	.78	.93	.93	1.00

BASALT

THE COVARIANCE AND MEAN FOR TRAINING CLASS BASALT

	500-600	600-700	700-800	800-1100
MEAN	31.91	46.38	52.06	41.32
ST DEV	2.46	4.73	5.21	5.41

COVARIANCE MATRIX

	500-600	600-700	700-800	800-1100
500-600	6.05			
600-700	9.72	22.36		
700-800	9.99	21.25	27.13	
800-1100	9.58	19.95	25.19	29.26

CORRELATION MATRIX

	500-600	600-700	700-800	800-1100
500-600	1.00			
600-700	.84	1.00		
700-800	.78	.86	1.00	
800-1100	.72	.78	.89	1.00

VEGETATION

THE COVARIANCE AND MEAN FOR TRAINING CLASS VEGETATION

	500-600	600-700	700-800	800-1100
MEAN	30.65	41.00	63.75	60.12
ST DEV	5.61	11.59	4.97	6.58

COVARIANCE MATRIX

	500-600	600-700	700-800	800-1100
500-600	31.45			
600-700	63.11	134.35		
700-800	14.55	28.48	24.73	
800-1100	-13.79	-31.21	15.70	43.32

CORRELATION MATRIX

	500-600	600-700	700-800	800-1100
500-600	1.00			
600-700	.97	1.00		
700-800	.52	.49	1.00	
800-1100	-.37	-.41	.46	1.00

COVARIANCES, MEANS, COVARIANCE MATRICES AND CORRELATION MATRICES FOR THE THREE GROUND FEATURES.

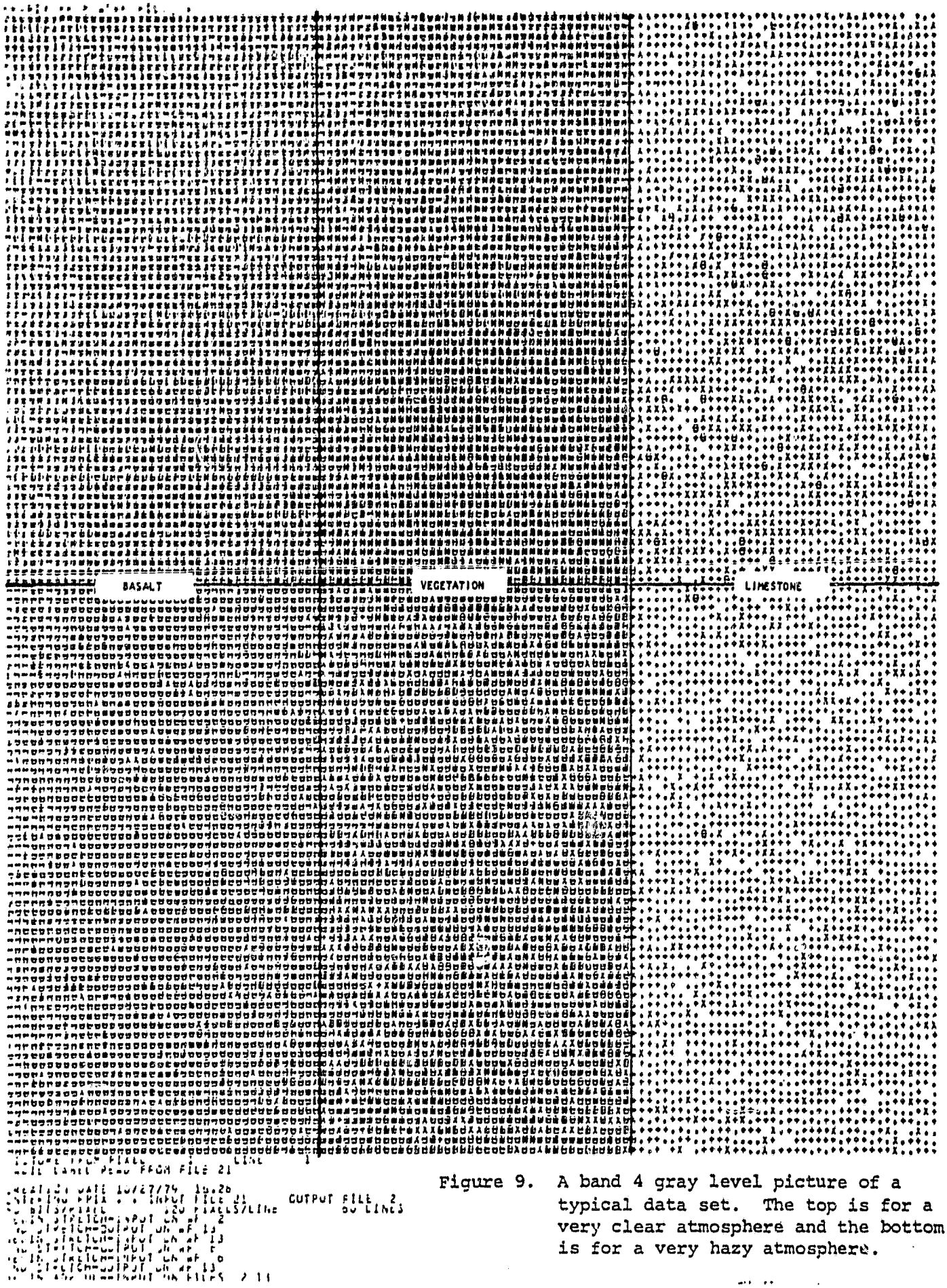

Figure 9. A band 4 gray level picture of a typical data set. The top is for a very clear atmosphere and the bottom is for a very hazy atmosphere.

of the pictures decrease as the atmosphere becomes more hazy. This effect is less noticeable in the case of limestone because it has a higher reflectance than the other surfaces.

The class statistics for the three atmospheric conditions are shown in Table 3. Note that the class means increase with increasing haze and that the increase is most noticeable for the lower reflectance surfaces. The standard deviations decrease as the atmosphere becomes more turbid. This again is due to a reduction in contrast or a compression in the gray level range.

LARSYS was used to classify the atmospherically degraded imagery. Figure 10 shows the result of training on the features under very clear atmospheric conditions and testing under hazy conditions. The errors in classification are seen to be greatest for basalt. This is due to basalt having the lowest reflectance of the three features and therefore its signature being modified most by changes in atmospheric conditions.

A second classification was made using LARSYS in which the training was performed under the hazy atmospheric conditions and the tests were conducted under the clear atmospheric conditions. The results are shown in Fig. 11 and it can be seen that the errors in classification, for the same change in atmospheric conditions as in the previous case, are less than those in Fig. 10.

The pictorial results illustrated in Figs. 10 and 11 are summarized quantitatively in Table 4, along with the results of other atmospheric changes. The first numerical column indicates the accuracy of the training site area. Three important conclusions can be drawn from Table 4:

1. The decrease in classification accuracy is greater the greater the change in atmospheric conditions unless the initial accuracy is very high when the accuracy can actually increase (see the limestone entry in Table 4).
2. The classification accuracy decreases the most for basalt, the lowest reflectance feature.
3. Except in the case of limestone, the classification accuracy decreases less with change in atmospheric conditions when the training is performed under poor atmospheric conditions and the testing is

TABLE 3

CLASS STATISTICS

	Mean			Standard deviation		
Band	Atm 0	Atm 1	Atm 2	Atm 0	Atm 1	Atm 2
Basalt						
4	31.9	33.8	37.4	2.46	2.41	2.22
5	48.4	49.1	51.2	4.73	4.81	4.65
6	52.1	52.9	52.9	5.21	5.15	5.07
7	41.3	41.9	42.5	5.41	5.44	5.21
Vegetation						
4	30.7	32.6	36.2	5.61	5.39	5.07
5	41.0	41.8	44.2	11.59	11.64	11.01
6	63.8	64.4	64.4	4.97	5.03	4.96
7	60.1	60.7	60.4	6.58	6.59	6.24
Limestone						
4	53.1	53.7	56.0	5.65	5.61	5.13
5	77.2	78.0	79.0	8.42	8.43	7.86
6	82.4	83.2	82.0	9.06	8.99	8.62
7	67.1	67.6	67.0	7.79	7.81	7.37

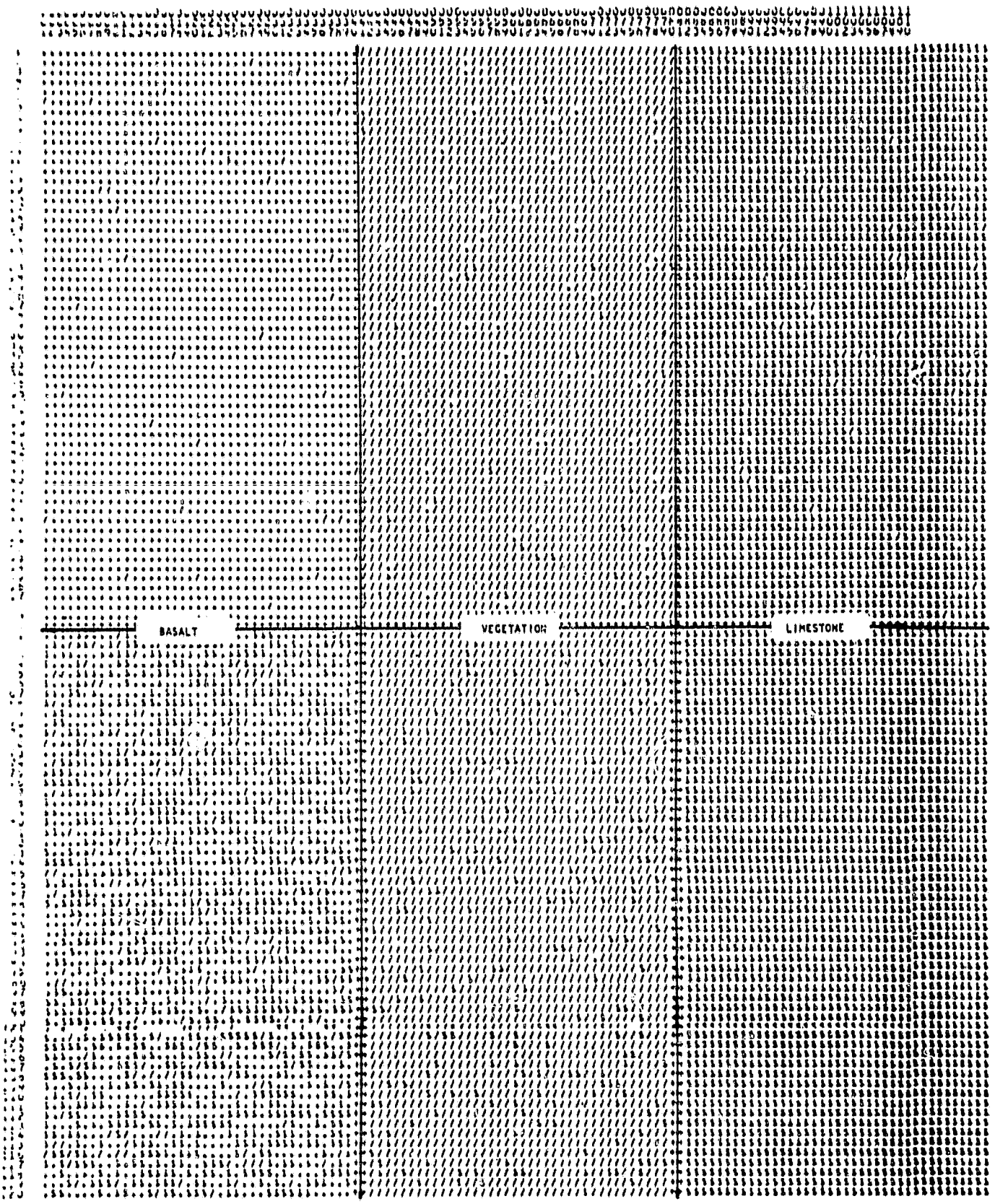

Figure 10. The result of a LARSYS classification using a clear atompshere (top) for the training conditions and a hazy atmosphere for the test conditions.

Figure 11. The result of a LARSYS classification using a hazy atmosphere (top) for the training conditions and a clear atmosphere for the test conditions

TABLE 4

CLASSIFICATION ACCURACIES

	ATMØ/ATMØ	ATMØ/ATM1	ATMØ/ATM2	ATM1/ATM2
BASALT	98.4	93.5	44.7	91.8
VEGETATION	96.1	95.7	89.3	92.0
LIMESTONE	98.6	99.5	100.0	99.8
AVERAGE	97.7	96.2	78.0	94.5

	ATM2/ATM1	ATM2/ATMØ	ATM1/ATMØ
BASALT	98.4	97.8	99.5
VEGETATION	95.0	93.3	94.3
LIMESTONE	93.8	92.7	97.2
AVERAGE	95.7	94.6	97.0

under good atmospheric conditions than vice versa. This phenomena has been reported by Potter and Shelton (1974) and Turner (1975).

4.0 THE TWO-WAVELENGTH APPROACH TO ATMOSPHERIC CORRECTION

In order to correct the spectral radiance at the entrance pupil of a sensor for atmospheric effects, we need to know the transmittance along the path from the ground feature to the sensor and the path radiance, i.e., the radiance detected by the sensor introduced by atmospheric scattering. In this and the next section we shall describe two different approaches to determining the atmospheric extinction coefficient, τ_{ext}, (related to transmittance, τ, by $\tau = \exp - \tau_{ext}$) and path radiance L_p.

The basis of the two-wavelength approach is as follows. If the total θ dependent radiances at the sensor at, for example, wavelengths 0.69 and 0.71 μm are L_{69} and L_{71}, the ground scene is Lambertian with a change in reflectance from ρ at 0.69 μm to $\rho + \Delta\rho$ at 0.71 μm then

$$L_{69} = \frac{E\rho}{\pi} \left(e^{-\overline{\tau} \sec\theta} \; e^{\Delta\tau \sec\Theta} \right) + L_\rho(\Theta)$$

$$\text{and} \quad L_{71} = \frac{E(\rho + \Delta\rho)}{\pi} \left(e^{-\overline{\tau} \sec\Theta} \; e^{-\Delta\tau \sec\Theta} \right) + L\rho(\Theta)$$

where $\overline{\tau}$ is the value of the extinction coefficient at 0.70 μm. The ground irradiance at the neighboring wavelengths is assumed the same. We can then subtract these equations to obtain

$$L_{69} - L_{71} = \frac{E\rho}{\pi} e^{-\overline{\tau} \sec\Theta} \left(e^{\Delta\tau \sec} - e^{-\Delta\tau \sec\Theta} - \frac{\Delta\rho}{\rho} e^{-\Delta\tau \sec\Theta} \right)$$

Taking the natural logarithm of both sides

$$\ln(L_{69} - L_{71}) = -\overline{\tau} \sec\Theta + \ln \frac{E\rho}{\pi} + \ln (\quad)$$

where the last brackets include the three terms in parentheses in the previous equation. Obviously, if the last two terms in this equation are independent of $\sec\Theta$ then the slope of a plot of $\ln (L_{69} - L_{71})$ versus $\sec\Theta$ will yield $\overline{\tau}$.

A typical result of this method is shown in the lower curve in Fig. 12.

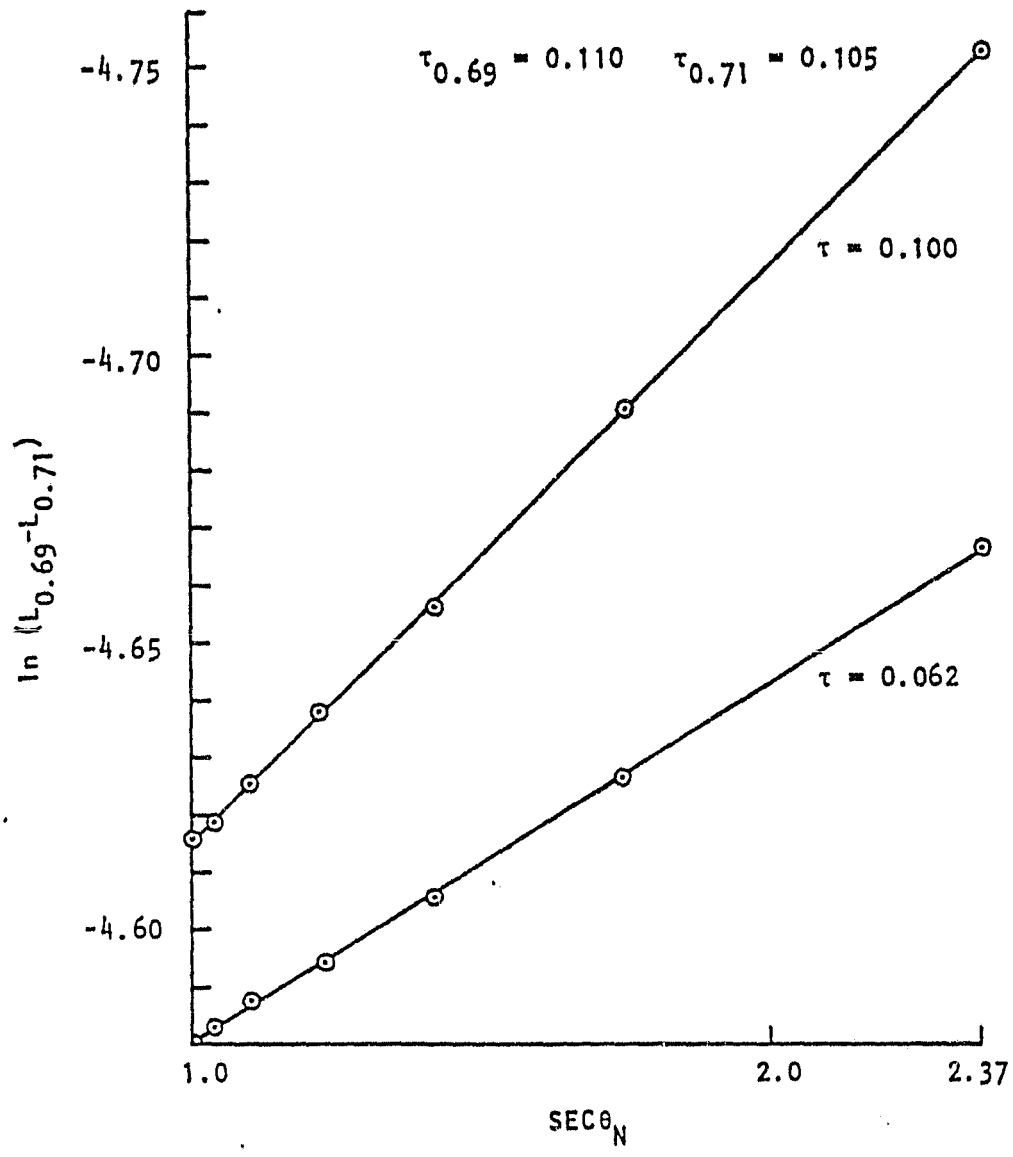

Figure 12. A plot of ln ($L_{0.69}$ - $L_{0.71}$) versus secθ, upper curve corrected for path radiance lower curve uncorrected for path radiance.

Model data were used of $\tau = 0.110$ at $\lambda = 0.69$ μm and $\tau = 0.105$ at $\lambda = 0.71$ μm. A change in reflectance, representative of vegetation, of 0.05 from 0.05 to 0.10 was also chosen. The curve of $\ln (L_{69} - L_{71})$ versus $\sec\Theta$ is a straight line with all the points falling close to the curve. Unfortunately, the slope of the curve yields a low τ value of 0.062. In order to determine the cause of the discrepancy in τ value, the value of L_p calculated from the model output were subtracted from the total radiance value of I_p at the sensor and the above procedure was repeated. The upper curve in Fig. 12 resulted, which gave a τ value very close to the correct mean value. This indicated that the problem lay in assuming the L_p values increased at the same rate with Θ as the total radiance values at the sensor. If in fact the L_p contributions did not cancel with subtraction, the total radiance and the path radiance for the two wavelengths and reflectances as a function of Θ are shown in Figure 13 and the difference in the slopes between the L_s and L_p curves is evident. Unfortunately, although the choice of reflectance and extinction values yielded a difference in L_s values twenty times larger than the difference in L_p values, the greater slope of L_p versus $\sec\theta$ strongly influences the estimated value for $\bar{\tau}$.

Other values of reflectance at $\lambda = 0.69$ and 0.71 μ m were tried and the results are listed in Table 5. These show that the values of the reflectances used do affect the accuracy of the estimate of $\bar{\tau}$ but this influence is overshadowed by the slope of the curve of L_p versus $\sec\theta$.

$\tau_{0.69} = 0.110, \quad \tau_{0.71} = 0.105$

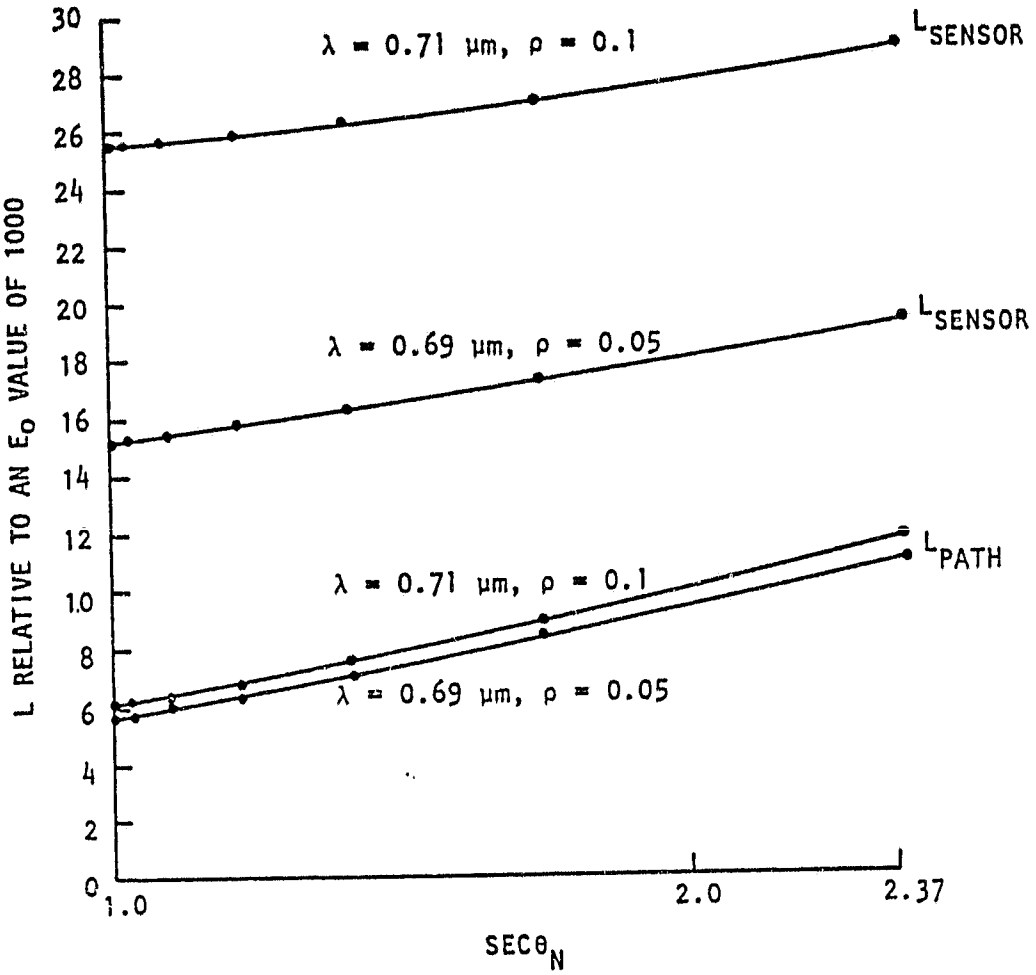

Figure 13. Plot of radiance versus secθ showing the non-parallelism of path and total radiance.

TABLE 5

τ VALUES AS CALCULATED BY THE TWO-WAVELENGTH METHOD

$\tau_{690} = 0.110$ $\tau_{710} = 0.105$

		ρ_{690} = 0.05	0.1	0.15	
ρ_{710}	0.1	0.061			τ values
	0.15	0.050	0.058		
	0.20	0.046	0.049	0.057	

5.0 A NUMERICAL PROCEDURE FOR DETERMINING τ, ρ, and L_ρ

The acquisition of radiometric measurements via a pointable-satellite-borne radiometer would provide nadir-angle dependent data, and consequently more information about the atmosphere. A numerical procedure to analyze these measurements will be discussed that will permit determination of optical depth (τ), path radiance (L_p), and ground reflectance, (ρ). This method simultaneously computes these parameters, effectively applying the atmospheric corrections during processing.

Mathematical Formulation

A non-linear regression procedure was utilized to fit nadir-angle dependent radiometric data to a theoretical expression describing the measurements. Radiative transfer calculations provided realistic data to test this method.

In general, the radiance at the entrance aperture of a pointable satellite-based radiometer for a specified spectral band is given by the expression

$$L_s\ (\Theta_N,\Theta_Z,\tau,\rho) = E_{tot}(\Theta_N,\Theta_Z,\tau,\rho)\ \frac{\rho(\Theta_N,\Theta_Z)}{\pi}\ \exp(-\tau\sec\ (\Theta_N)) + L_\rho(\Theta_N,\Theta_Z,\tau,\rho) \quad (1)$$

where the functional dependencies of the quantities are indicated.
The quantities involved are:

L_s : Radiance at the sensor

E_{tot} : Total irradiance at the ground

$$E_{tot} = E_o\ \cos\ (\Theta_Z)\ \exp\ (-\tau\sec\ (\Theta_Z)) + E_D \quad (2)$$

E_o : Extraterrestial solar irradiance in spectral bands

E_D : Diffuse sky irradiance at ground

τ : Total atmospheric optical depth

Θ_N : Nadir angle

Θ_Z : Solar zenith angle

ρ : Ground reflectance

L_p : Path radiance

The quantities τ, ρ, and L_p need to be known in order to analyze the ground scene. Unfortunately, this is a problem of at least four unknown E_D, τ, ρ, and L_p, with and L_p having an additional angular dependence. A series of measurements of L_s as a function of Θ_N will not analytically resolve this inadequately specified problem, except for the nonrealistic case of $\tau = 0$ where $L_p = 0$ and $E_D = 0$. Combining information from various spectral bands may produce an analytic result with less severe constraints on τ, but would require knowledge about the spectral character of E_D, τ, ρ, and L_p. These spectral characteristics, however, could only be derived from information about or apriori assumptions regarding the atmosphere.

Given a set of L_s (Θ_N) values, the unknowns can be determined by a non-linear regression technique if the angular dependencies of ρ and L_p can be specified. Model atmosphere radiative transfer calculations of L_s and L_p revealed a simple functional dependence for L_p. The radiative transfer analysis (Herman, 1975) assumed a plane parallel atmosphere and a uniform Lambertian reflectance. For the representative conditions of a solar azimuth angle of 90^0 and zenith angle of 45^0 the model calculations show L_p to be a linear function of exp $(-\tau \sec \Theta_N)$, Fig. 14. Therefore, for a given τ, ρ, and fixed Θ_Z, we can expand L_p, such that

$$L_p\ (\Theta_N) = \alpha - \beta \exp\ (-\tau \sec \Theta_N) \qquad (3)$$

Note that this linear relationship holds only for solar zenith angles near 90^0. For other angles a simple polynominal expression (probably quadratic) is necessary.

The angular variation of ρ could be included by parameterizing the appropriate bidirectional reflectance distribution function (BRDF) for the type of scene viewed. However, the ultimate goal in this analysis was to determine if the numerical technique could predict the radiative transfer calculation values for inputs τ, ρ and outputs E_D, L_p. Since the radiative transfer computation assumed a constant ρ, a BRDF was not incorporated in the numerical analysis, but it could be accommodated.

Therefore, with the above assumptions regarding the angular dependencies, equations 1-3 can be combined to give a general theoretical expression and representation of the results of the radiative transfer

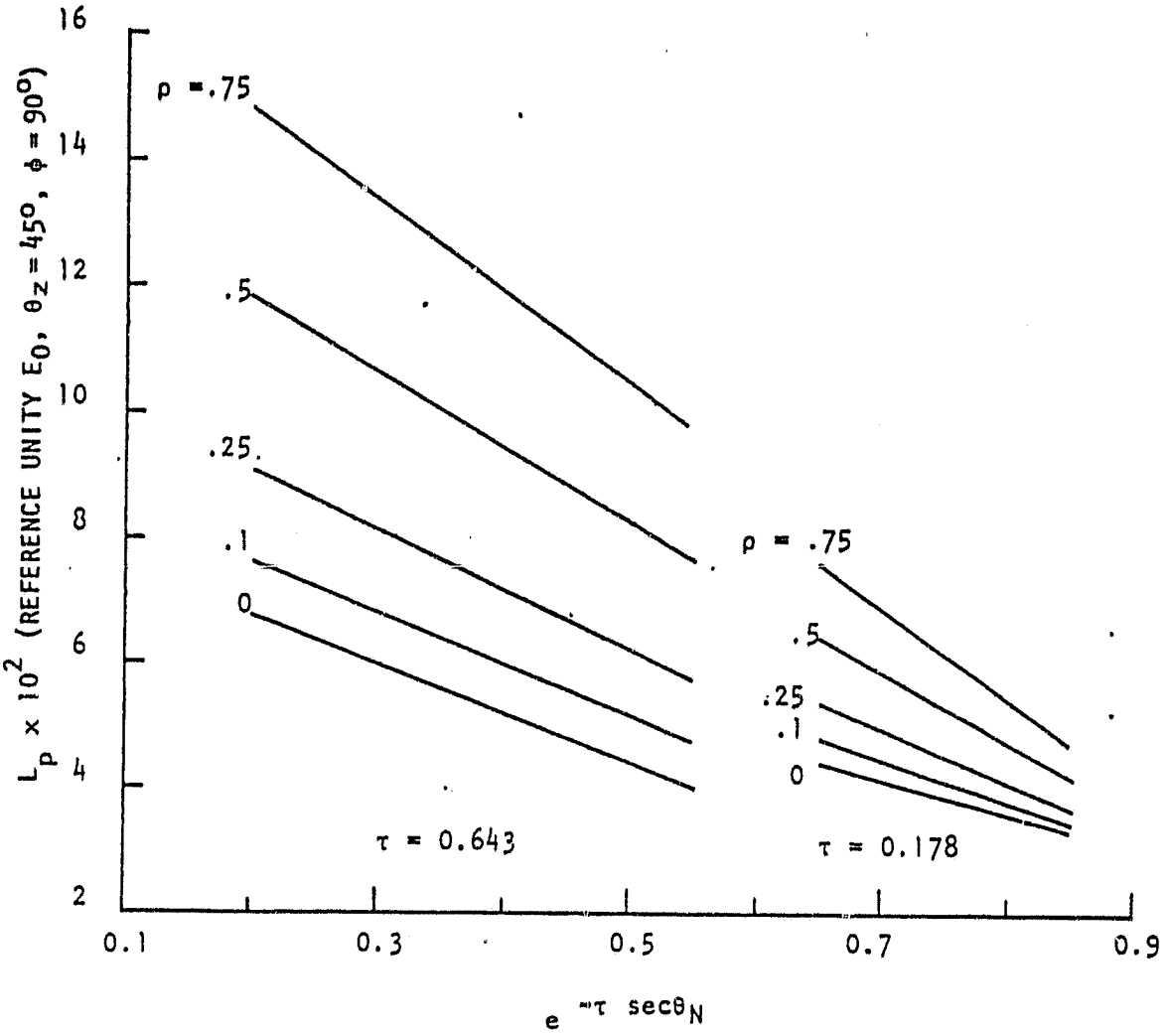

Fig. 14. Plots of path radiance, L_p, versus $\exp(-\tau \sec\theta_N)$ for λ = 500 nm, τ = 0.178, 0.643, and ρ = 0, 0.1, 0.25, 0.5, 0.75. Note the linear character of these plots for the choice of a solar zenith angle of 45° and azimuth angle of 90°.

calculations for the total radiance at the sensor as a function of nadir angle.

$$L_s(\Theta_N) = \alpha + \left[\frac{1}{\pi}\ (E_o \cos\Theta_Z \exp(-\tau\ \sec\Theta_Z) + E_D) - \beta\right] \exp(-\tau\ \sec\Theta_N) \qquad (4)$$

5.1 Non-Linear Regression Technique

Equation (4) can be rewritten as a non-linear expression of unknown parameters a_j for a range of nadir angles Θ_i (the N subscript will be suppressed, but implicit)

$$L_s(\Theta_i) = a_4 + \left[\frac{a_2}{\pi}\ (E_o \cos\Theta_Z\ \exp(-a_1 \sec\Theta_Z)\ + a_5\right]\ \exp(-a_1 \sec\Theta_i) \qquad (5)$$

where $a_1 = \tau$, $a_2 = \rho$, $a_3 = E_D$, and a_4, a_5 determine L_ρ. Given a set of measured values, L_{si}, as a function of Θ_i and uncertainties, σ_i, in the data points L_{si}, a non-linear regression technique can optimize the choice of parameters a_j by minimizing χ^2, where

$$\chi^2 = \sum_i \left\{ \frac{1}{\sigma_i^2} \left[L_{si} - L_s\ (\Theta_i)\right]^2 \right\} . \qquad (6)$$

This estimate of the parameters, a_j, will determine the most probable functional form of $L_s(\theta_i)$ that will fit the data L_{si} and consequently give an estimate for τ, ρ, and L_p.

The regression analysis estimates the parameters by minimizing χ^2 with respect to each of the parameters simultaneously,

$$\frac{\partial}{\partial a_j}\ \chi^2 = \frac{\partial}{\partial a_j} \sum \left\{ \frac{1}{\sigma_i 2} \left[L_{si} - L_s(\theta_i)\ \right]^2 \right\} = 0. \qquad (7)$$

Since $L_s(\Theta_i)$ is a function of five parameters, this method finds the minimum of χ^2 in a five-dimensional hyperspace. The numerical technique utilized to accomplish this search of the hypersurface was first suggested by Marquardt (1963) and coded in Fortran by Bevington (1969).

The Marquardt approach probes the hypersurface by determining the gradient of the surface given an initial set of parameters, a_j, and parameter increments δa_j. The a_j values are then incremented following the path of steepest descent to the region of a minimum. Near the minimum the function $L_s(\theta_i)$ is expanded in a first-order Taylor's expansion, linear in the parameter increments δa_j. Substituting the expansion into Eq. (7) and taking the derivative numerically generates a set of five simultaneous equations. The equations are then solved by linear regression matrix techniques to determine the optimum set of increments δa_j to augment the parameter values to correspond to those at the hypersurface minimum. The process is repeated until the χ^2 value changes by less than a specified amount between iterations. The procedure then computes the uncertainties σa_j, in the determined best fit parameter values, a_j.

Considering the above steps in detail, the first-order Taylor expansion in parameters a_j can be written:

$$L_s(\theta_i) = L_{so}(\theta_i) + \sum_j \left[\frac{\partial L_{so}(\theta_i)}{\partial a_j} \delta_j \right] \tag{8}$$

which is linear in δa_j. L_{so} and the derivatives are evaluated with the initial a_j values.

The derivatives are computed numerically for a given Θ_1 value,

$$\frac{\partial L_{so}(\theta_i)}{\partial a_j} = \frac{1}{2\Delta a_j} \left[L_s(a_j + \Delta a_j) - L_s(a_j - \Delta a_j) \right] \tag{9}$$

where Δa_j is the non-optimized initial input guess for the parameter increments δa_j. Substituting equation (8) into equation (6) yields

$$\chi^2 = \sum_i \left\{ \frac{1}{\sigma^2_i} \left[L_{si} - L_{so}(\theta_i) - \sum_j \frac{\partial L_{so}(\theta_i)}{\partial a_j} \delta a_j \right]^2 \right\} . \tag{10}$$

In order to minimize this linear regression problem with respect to the parameter increments δa_j, expression (10) is differentiated,

$$\frac{\partial \chi^2}{\partial \delta a_k} = -2\sum_i \left\{ \frac{1}{\sigma_i^2} \left[L_{si} - L_{so}(\theta_i) - \sum_j \left(\frac{\partial L_{so}(\theta_i)}{\partial a_j} \delta a_j \right) \right] \frac{L_{so}(\theta_i)}{\partial a_k} \right\} = 0, \quad (11)$$

such that for a given θ_i,

$$L_{si} - L_{so}(\theta_i) = \sum_j \left(\frac{\partial L_{so}(\theta_i)}{\partial a_j} \right) \delta a_j. \quad (12)$$

Letting $\beta_k = -\frac{1}{2} \frac{\partial \chi^2}{\partial \delta a_k}$, equation (11) can be recast as the matrix relation,

$$\beta_k = \sum_j \delta a_j \, \alpha_{jk} \quad (13)$$

where

$$\alpha_{jk} = \sum_i \frac{1}{\sigma_i^2} \frac{\partial L_{so}(\theta_i)}{\partial a_j} \frac{\partial L_{so}(\theta_i)}{\partial a_k}. \quad (14)$$

Finally, solving the matrix relation

$$\underset{\sim}{\beta} = \delta \underset{\sim}{a} \, \underset{\approx}{\alpha} \quad (15)$$

for $\delta \underset{\sim}{a}$ will give the array of optimum increment values ∂a_j.

In order that this matrix method will quickly locate a minimum in the χ^2 hypersurface, Marquardt suggested the modification

$$\underset{\sim}{\beta} = \delta \underset{\sim}{a} \, \underset{\approx}{\alpha}' \quad (16)$$

where

$$\underset{\approx}{\alpha}' = \begin{matrix} \alpha_{jk}(1 + \lambda) & j = k \\ \alpha_{jk} & j \neq k \end{matrix}. \quad (17)$$

This alteration of the diagonal elements by the addition of λ serves a useful purpose. For λ small,

$$\underset{\approx}{\alpha} \approx \underset{\approx}{\alpha}' \quad (18)$$

and the solution obtained for the $_j$ values is that of the Taylor expansion. For λ large, the diagonal terms dominate

$$\beta_j \approx \lambda \delta_j \, a_{jj} \quad (19)$$

and the δa_j values increment a_j along a scaled gradient toward the minimum.

Therefore, the non-linear regression algorithm combines a gradient search with an analytical solution developed from linearizing the fitting function given by

$$\underset{\sim}{\delta a} = \underset{\sim}{\beta}\ \underset{\approx}{\varepsilon}', \tag{20}$$

where $\underset{\approx}{\varepsilon}'$ is the inverse of matrix $\underset{\sim}{\alpha}'$.

Finally, the standard deviation of the computed parameters a_j can be shown to be related to the square root of the diagonal elements ε'_{jj}.

The algorithm is implemented in an iteration procedure. The program searches for a λ value for the initial choice of $\underset{\sim}{a}$ such that $\chi^2(\underset{\sim}{a} + \delta\underset{\sim}{a}) < \chi^2(\delta\underset{\sim}{a})$. The array $\underset{\sim}{a}$ is then set equal to $\underset{\sim}{a} + \delta\underset{\sim}{a}$ and the analysis is repeated until λ, or the change in χ^2 between iterations is less than a preselected value.

The subroutine CURFIT (Bevington, p. 237) was utilized to perform a single λ iteration. A listing of the FORTRAN computer code SKYRAD which utilized CURFIT in the regression technique analysis is contained in Appendix A. The program consists of the main program which input/output's the data, and calls the subroutines CURFIT, FUNCT, FDERIV, SCHISQ, and MXINV, and evaluates the results.

The main program and subroutines are sufficiently documented to understand their operation. Comment cards in the main program describe the input data arrangement necessary to run the code.

A brief description of the routines are:

SKYRAD : Main Program

CURFIT : Non-linear Regression subroutine described

FUNCT : Evaluates Eq. (5) at θ_i for a given set of a_j values

FDERIV : Evaluates the derivatives in Eq. (5) numerically via Eq. (9) at each point θ_i with respect to each parameter a_j.

SCHISQ : Evaluates the reduced χ^2 value for a given set of data and fit parameters a_j

MXINV : Evaluates the inverse of the $\underset{\sim}{\alpha}'$ matrix.

A typical output of the SKYRAD is contained in Appendix B.

Evaluation of the Effectiveness of the Regression Code

In order to evaluate the efficiency and accuracy of the non-linear regression technique in computing the parameters before analyzing model atmosphere radiative transfer results, the program SYNRAD was written to synthesize data sets as inputs to SKYRAD. For a given representative choice of a_j and θ_i, SYNRAD computed the array $L_s(\theta_i)$ using Eq. (5) and the corresponding array of σ_i values for a specified amount of random noise added to $L_s(\theta_i)$. The arrays θ_i, $L_s(\theta)$, and σ_i were then stored as the input file TAPE5 for the code SKYRAD.

The ability to exactly specify the input parameters of the synthesized data permitted examination of the following areas:

1) Number and range of input θ_i values necessary

2) Effect of input choices on the convergence and output of SKYRAD

3) Independence of the a_j parameters and their effect on $L_s(\theta_i)$

4) Effect of random noise on convergence

5) Curvature of the χ^2 five-dimensional hypersurface.

This test approach provided useful familiarity with the operation of SKYRAD and the characteristics of the $L_s(\theta)$ expression, Eq. (5). This understanding led to a procedure with which to analyze the $L_s(\theta_i)$ data from the model calculations.

Graphical examination of Eq. (5) for various choices of the input parameters revealed that the ρ parameter strongly influences the shape and curvature of the $L_s(\theta_i)$ data. This fact will be utilized in the next section. Four representative cases were consequently examined including the investigation of the range of θ_i values. The parameter combinations considered were:

τ (a_1)	E_D (a_3)	L_p (a_4, a_5)	ρ (a_2)	θ_i Range
0.2	0.2 E_o	0.15 E_o	0.1	0^o - 60^o
				0^o - 45^o
			0.5	0^o - 60^o
				0^o - 45^o

The synthetic data generated with these parameters were analyzed with SKYRAD for various choices of input parameters a_j.

The choice of sixteen evenly spaced data points, θ_i, gives the program eleven degrees of freedom with which to search for a solution that can be accepted with reasonable confidence. This number of points also permits an adequate sampling of nadir values. There was no significant difference in SKYRAD outputs for identical cases of input parameters with either choice of θ_i range. Therefore, the restricted range, $0^o \leq \theta_i \leq 45^o$, was chosen because for this range the ground-projected instantaneous field of view (IFOV) is smaller and the plane parallel atmosphere assumption of the atmospheric model radiative transfer computations is not seriously violated.

To evaluate the effect of the first iteration initial guess of input parameters, a_j, a series of twenty-five input selections were evaluated for each set of synthesized data. A range of values for a given a_j were input holding the other parameters a_k, $j \neq k$, constant at the model values. Typically, each trial converged in three to ten iterations.

The results of systematic parameter variation analysis are:

a_1: If τ is overestimated, SKYRAD will converge to the correct solution but takes many iterations, 20-30. If τ is underestimated the code will converge, but a_5 is changed to compensate and the predicted L_p tends to be low.

a_2: The solution SKYRAD predicts is very dependent on the choice of ρ.

a_3: The convergence of SKYRAD is very insensitive to variations in E_D.

a_4, a_5: The SKYRAD output is very dependent on the input value of L_p converging poorly for an overestimated L_p input.

a_j: If all the parameters are systematically varied, either all substantially too large or too small, SKYRAD fails to converge or converges poorly.

Therefore, a judicious choice of input parameters is necessary to effectively use this numerical technique.

The results of this investigation revealed significant details about the functional dependance of $L_s(\theta_i)$ on the a_j parameters and the curvature of the χ^2 hypersurface. The parameters of a_j are not strictly mathematically independent in their effects on the shape of $L_s(\theta_i)$. Variations in one parameter can be compensated for by variations in other parameters without significantly altering the curvature. In effect, the curvature of L_s vs θ_i is not uniquely determined by a single choice of $\underset{\sim}{a}$. Consequently, the χ^2 hypersurface is not characterized with a major deep minimum, but rather can be imagined as being bumpy with minor local minima, which SKYRAD can interpret as a solution.

The fact that SKYRAD can converge to a number of equally acceptable solutions via the χ^2 condition is disconcerting, but additional knowledge about the dependence of E_D and L_p on τ and ρ enables a judicious evaluation of these solutions. The procedure necessary to effectively utilize the regression analysis will be discussed in the later section dealing with data from the model atmosphere radiative transfer calculation.

An additional means of avoiding undesirable solutions was to prevent SKYRAD from predicting negative values for any of the a_j parameters, since only positive values are allowable given the form of Eq. (5). The subroutine CURFIT was modified to prevent determination of negative a_j values for any iteration.

The effect of random noise added to the $L_s(\theta_i)$ data was considered. The presence of up to 0.1% random noise did not prevent the convergence of SKYRAD to acceptable solutions. The presence of 1% random noise began to affect the fits to the synthesized data if $\rho \sim 0.5$, when $L_s(\theta_i)$ data had little curvature. The net result of this analysis is to suggest that the instrument have a signal to noise ratio, SNR > 100.

Non-Linear Regression Analysis of Model Data

In an effort to test the accuracy with which the numerical method could analyze real data, the output of radiative transfer calculations on model atmospheres was used as simulated "real" data input for the SKYRAD program.

Sets of $(\theta_i, L_s(\theta_i))$ data were compiled for specified wavelengths, but the τ and ρ values were unknown to the processor.

The radiative transfer computations were performed using the numerical approach described and coded by Herman and Browning. These calculations incorporated various model atmospheres of varying amounts of aerosol loading as suggested by Elterman.

For a fixed solar zenith angle of 45^{o}, a unit solar irradiance, E_o, and a uniform Lambertian reflectance, the path radiance and the radiance at the sensor (L_p, L_s) were computed for a range of reflectances and nadir and azimuth angles. These calculations also permitted determination of E_D for each τ, ρ combination. The computations were performed for wavelength values of 380, 500, 650, 750, and 900 nm. The optical depth for each wavelength was determined by the model atmosphere and amount of aerosol loading. A thin and thick aerosol optical depth were chosen for each wavelength. The major cases considered are listed below.

λ	380		500		650		750		900		
τ RAY	.450		.145		.026		.023		.013		
τ MIE	.045	.669	.033	.498	.048	.397	.027	.344	.020	.300	
τ TOTAL	.495	1.119	.178	.643	.074	.445	.050	.371	.033	.313	

A typical computer output (λ = 500 nm, τ = 0.643) is contained in Appendix C.

Figures 15, 16, and 17 are plots of the radiative transfer calculation outputs, $L_s(\theta_i)$ is very reflectance dependent. As ρ increases the proportion of measured reflected signal increases and begins to dominate and the slopes of the plots change sign. As a result, the desirable type of scene from which to obtain data to process is one viewed through a thicker atmosphere with low ground reflectance. The $L_s(\theta_i)$ data for this type of scene has greater curvature, increasing the amount of parameter independence, and reducing the number of local minima in χ^2 space. The worst case is that for $\rho \sim 0.5$ where SKYRAD could attempt to fix a complicated function to a set of data which is nearly a straight line.

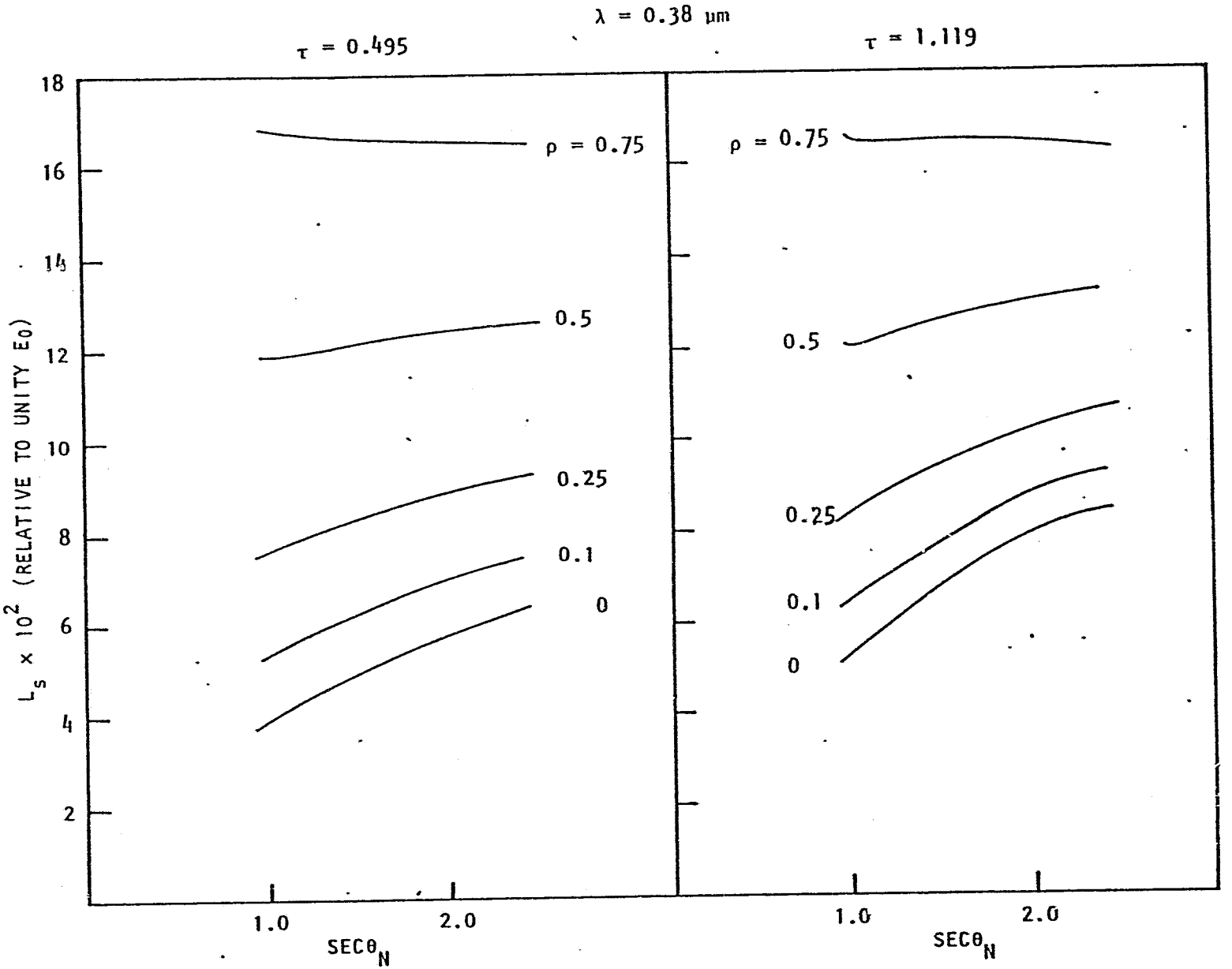

Fig. 15. Plots of the total sensor radiance, L_S, versus the secant of the nadir angle, $sec\theta_N$ for ρ = 0, 0.1, 0.25, 0.5, and 0.75, and λ = 380 nm.

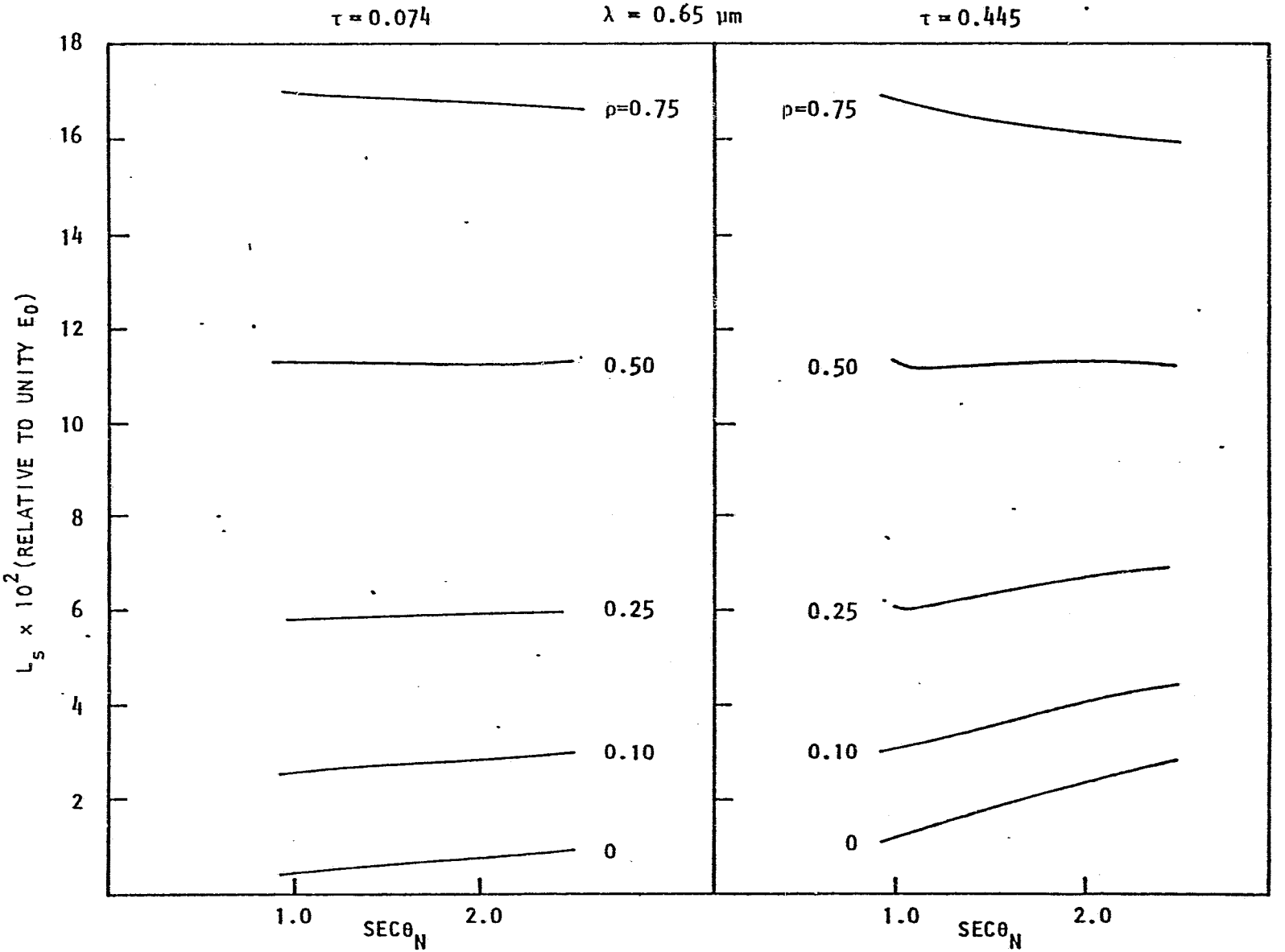

Fig. 16. Plots of the total sensor radiance, L_S, versus the secant of the nadir angle, secθ_N, for ρ = 0, 0.1, 0.25, 0.5, and 0.75, and λ = 650 nm.

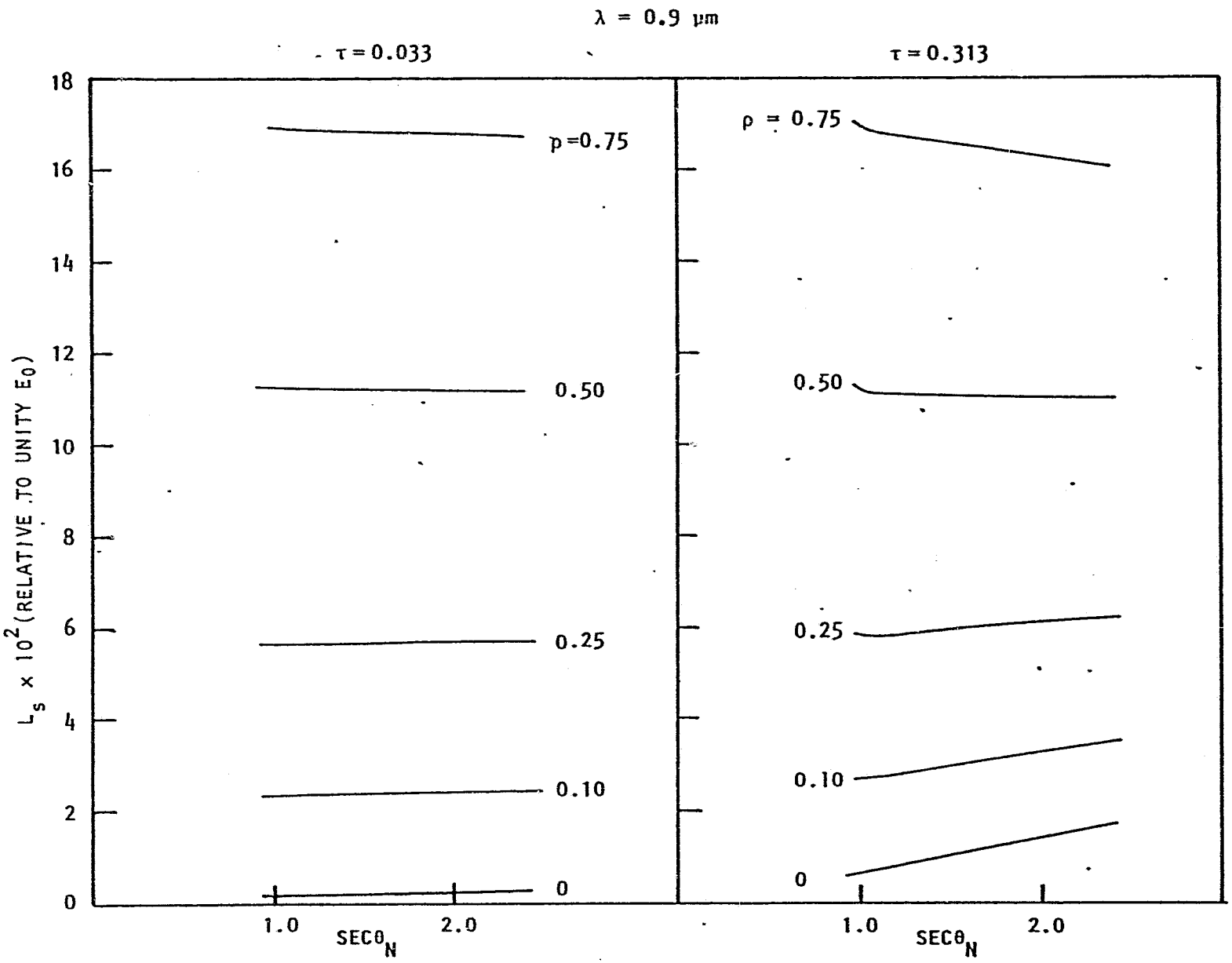

Fig. 17. Plots of the total sensor radiance, L_S, versus the secant of the nadir angle, secθ_N, for ρ = 0, 0.1, 0.25, 0.5, and 0.75, and λ = 900 nm.

Figures 20 and 21 are plots of the path radiance at the sensor, L_p, vs ρ for the models considered.

An important characteristic to notice in Figures 18-21 is that for a given τ and ρ value, the corresponding values of E_D and L_p are uniquely determined. This fact will be utilized later in the procedure for selecting input choices for the a_j parameters and evaluating the results predicted by SKYRAD.

Finally, a least squares straight line fit was made to $L_p(\theta_i)$ vs $\exp(-\tau \sec\theta_i)$ determining a_4 and a_5 for all the wavelength optical depth cases considered and these were tabulated along with the computed E_D values. This permits estimation of E_D and L_p for a given choice of λ, τ, and ρ.

Fitting Procedure for Numerical Technique

The model atmosphere radiative transfer calculations were used to provide unknowns for analysis by the non-linear regression method. An unknown was a data set of $L_s(\theta_i)$ values that was obtained from the model calculation output for an azimuth angle of 90^o. The wavelength of the data was provided, but not the optical depth or reflectance value. This was done in an attempt to simulate the realistic case of actual measured data. The goal was to utilize the numerical analysis method described to reproduce the initial τ and ρ values of the model case and predict E_D and L_p.

The experience gained analyzing the data of SYNRAD demonstrated that due to the bumpy nature of the χ^2 hypersurface an arbitrary choice of input parameters cannot be expected to converge to the correct result nor can a series of inputs be expected to converge to the same result. Therefore, a procedure was devised to judiciously determine a range of likely input parameters, to evaluate the subsequent outputs, refine the inputs and select a final result.
Procedure:

1) Select θ_1 points for $L_s(\theta_1)$ data and plot vs $\sec\theta_1$
2) Compare plot of $L_s(\theta_i)$ with curves from model calculations
   (a) From overall magnitude of $L_s(\theta_i)$ estimate likely range of τ, (a_1)
   (b) From overall curvature of $L_s(\theta_i)$ estimate likely range of ρ, (a_2)
3) For range of τ, ρ, from model calculation tables

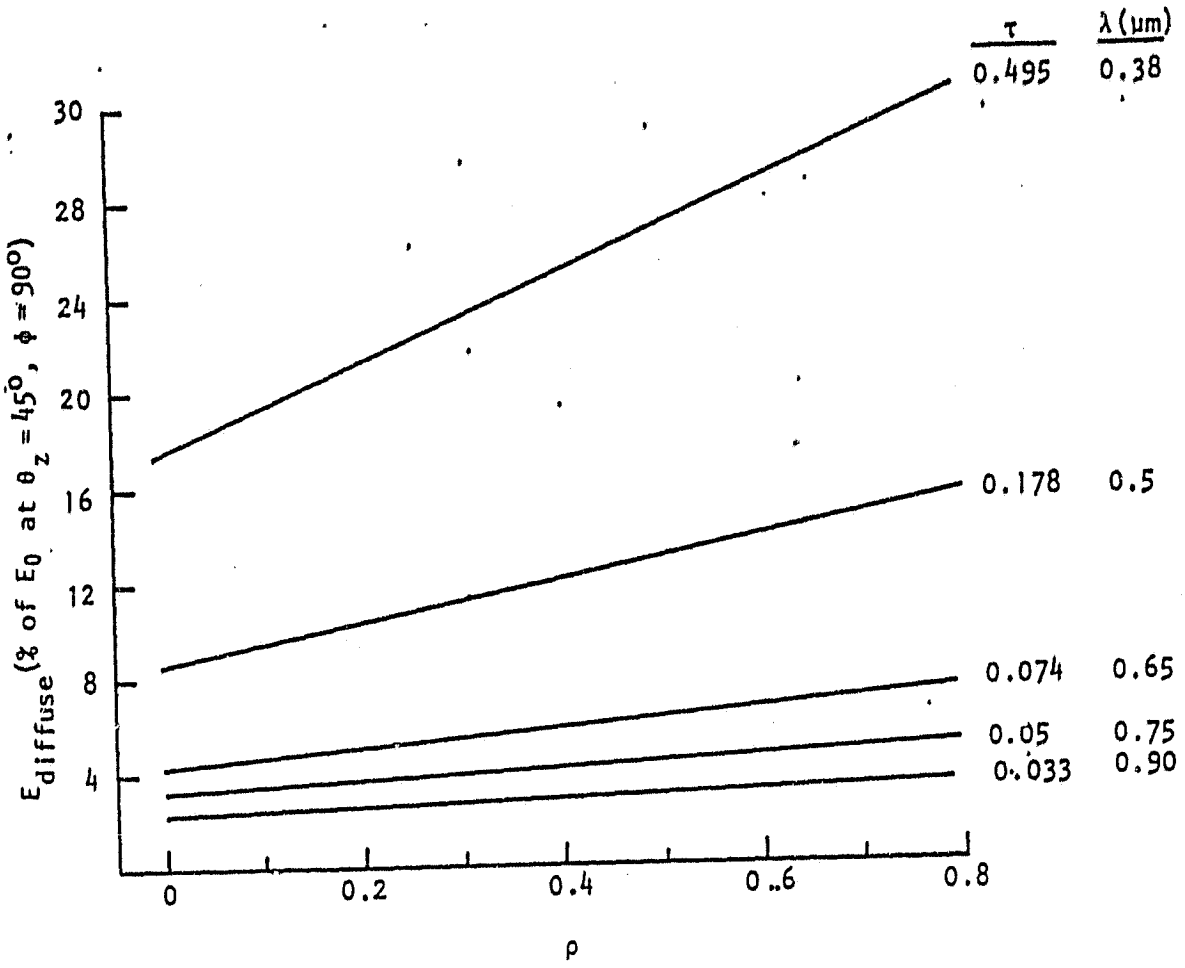

Fig. 18. Plots of the diffuse irradiance at the ground, E_D, versus reflectance, ρ, for the thin optical depth cases at the specified wavelengths. Note the systematic increase in slope and magnitude.

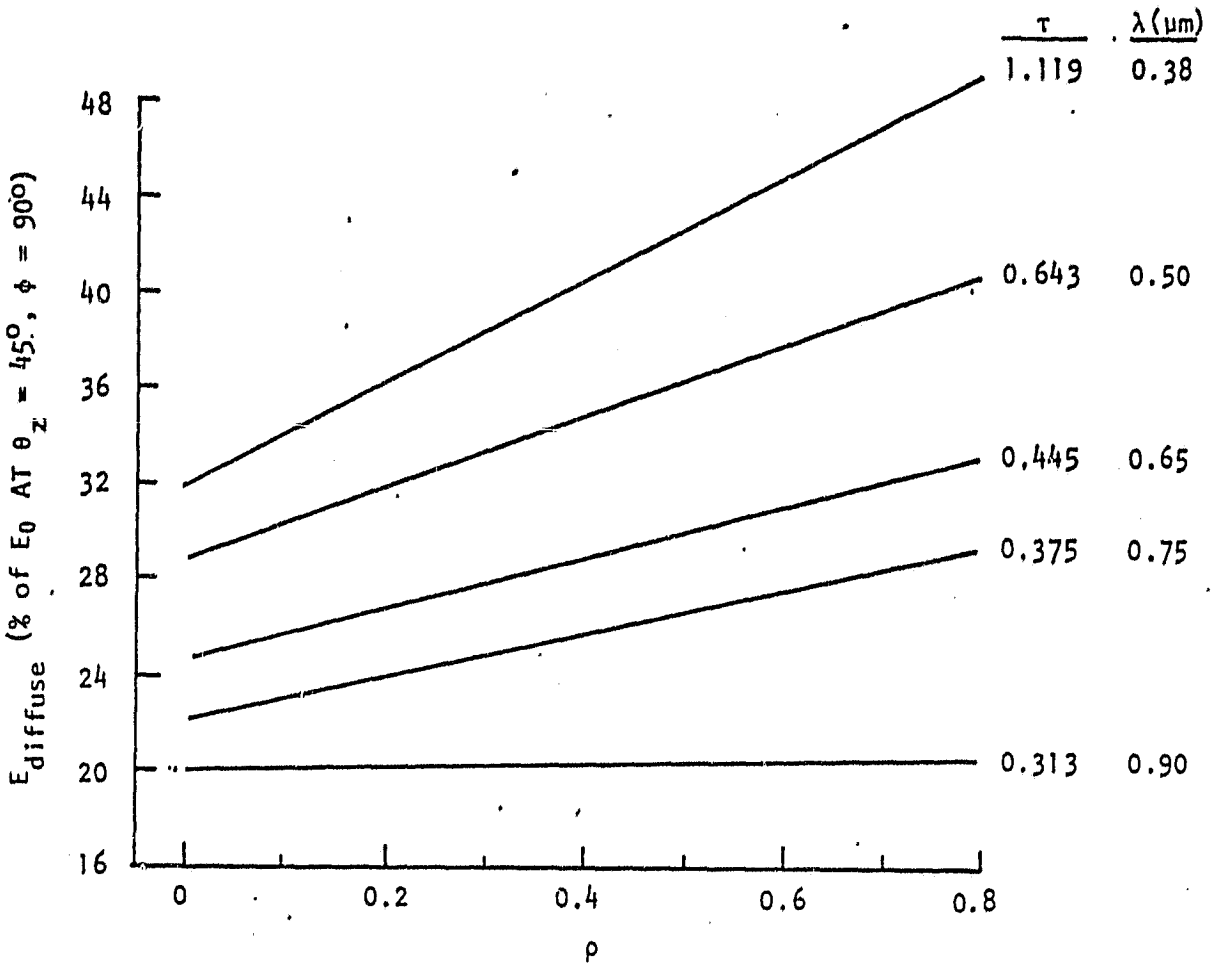

Fig. 19. Plots of the diffuse irradiance at the ground, E_D, versus reflectance, ρ, for the thick optical depth cases at the specified wavelengths. Note the systematic increase in slope and magnitude.

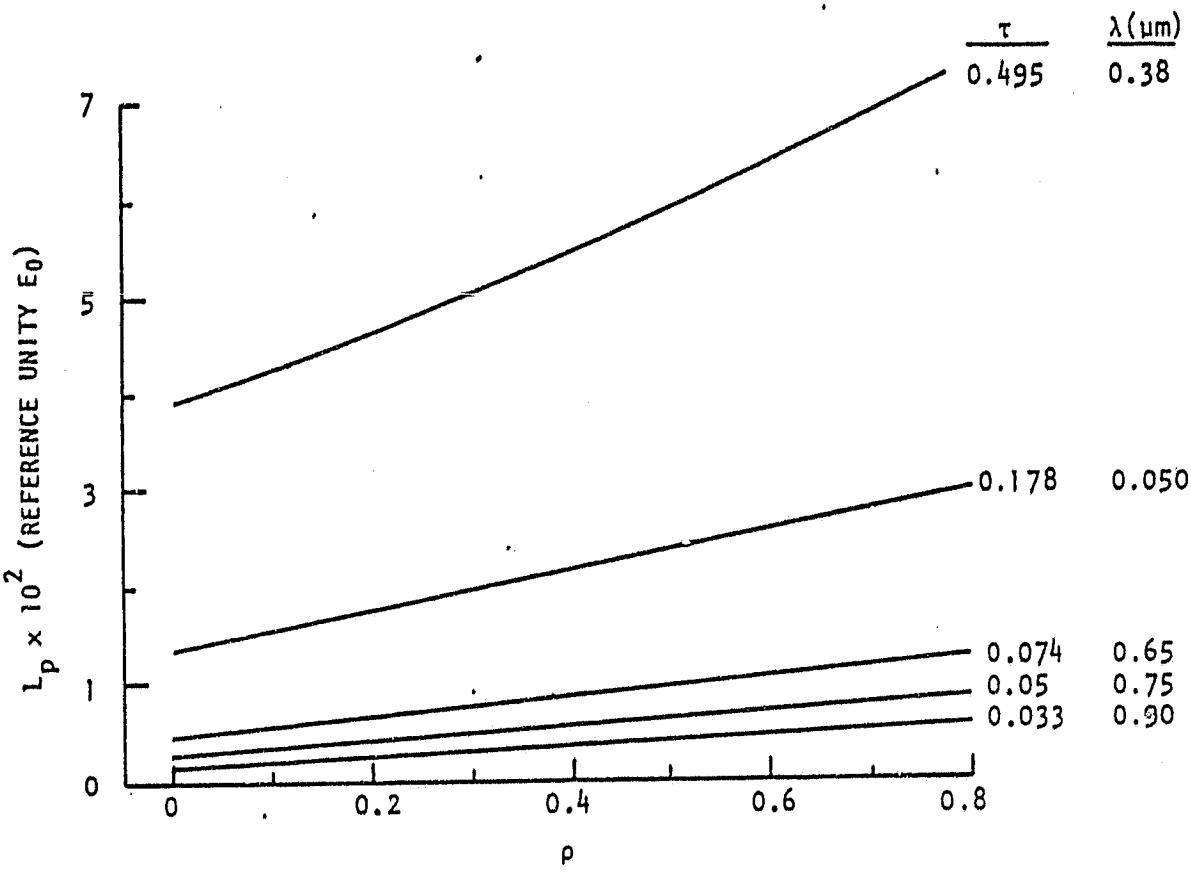

Fig. 20. Plots of path radiance, L_p, versus reflectance, ρ, for the thin optical depth cases at the specified wavelengths. Note the systematic increase in slope and magnitude.

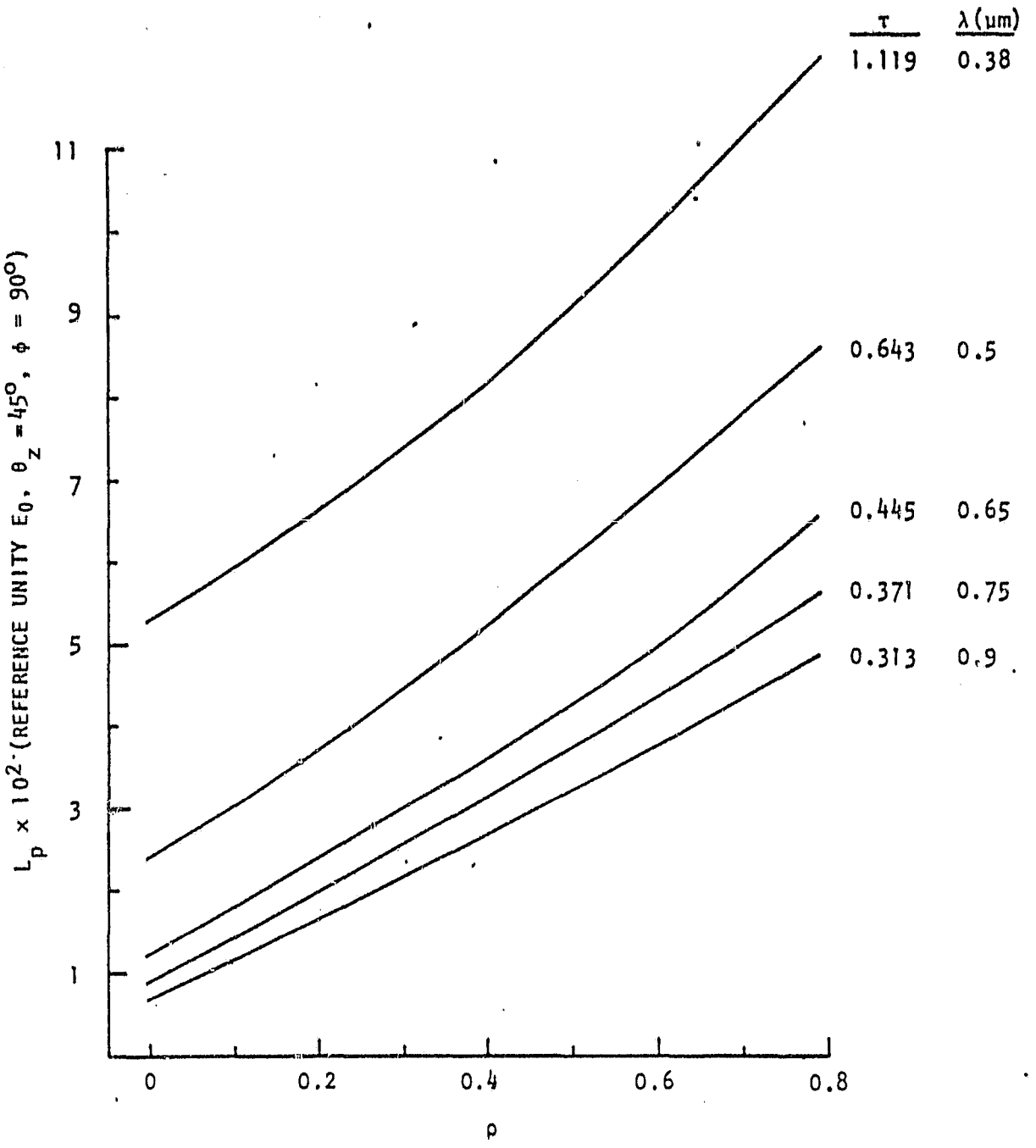

Fig. 21. Plots of path radiance, L_p, versus reflectance, ρ, for the thick optical depth cases at the specified wavelengths. Note the systematic increase in slope and magnitude.

(a) Estimate range of E_D, (a_3)

(b) Estimate range of L_p, (a_4, a_5)

4) Run SKYRAD for the selected range of input parameters
5) Evaluate results and refine input parameters
6) Run SKYRAD for the selected range of input parameters
7) Select result

Figure 22 illustrates the input and computed output $L_s(\theta_i)$ values of this procedure for one of the unknowns considered. The selection of data points from the model calculations was not uniform, but concentrated points by interpolation in the θ_i range, $15^o < \theta_i < 45^o$, in order to emphasize the curvature in the input data.

The initial range of parameter estimates were:

τ : $0.15 < a_1 < 0.25$

ρ : $0.05 < a_2 < 0.15$

E_D: $0.085 < a_3 < 0.095$

L_p: $.070 < a_4 < 0.075$

: $.065 < a_5 < 0.070$

The criterion for evaluation of the SKYRAD parameter predictions were:

1. Is the reduced χ^2 value reasonable?
2. Is the predicted value for τ reasonable?
   ($\tau > \tau_{RAYLEIGH}$)
3. Is the value for E_D reasonable?
   (SKYRAD tends to predict E_D with a large uncertainty, but pathological cases $E_D > 0.35E_o$ or $E_D < 0.01E_o$) are still rejectable)
4. Are the computed values of E_D and L_p consistent with the computed values for τ, ρ?
5. Langley plot ($\ln (L_s(\theta_i) - L_p(\theta_i)$ vs $\sec\theta_i$) the input data with the predicted path radiance subtracted. Does the slope of this plot equal the predicted τ value?

Approximately five sets of input parameters selected from the estimated ranges were run. The criteria above were used to evaluate the resulting SKYRAD predictions and define three refined sets of parameter inputs. The outputs were again evaluated and the input parameters narrowed to those of the final result tabulated here and plotted in Figure 22.

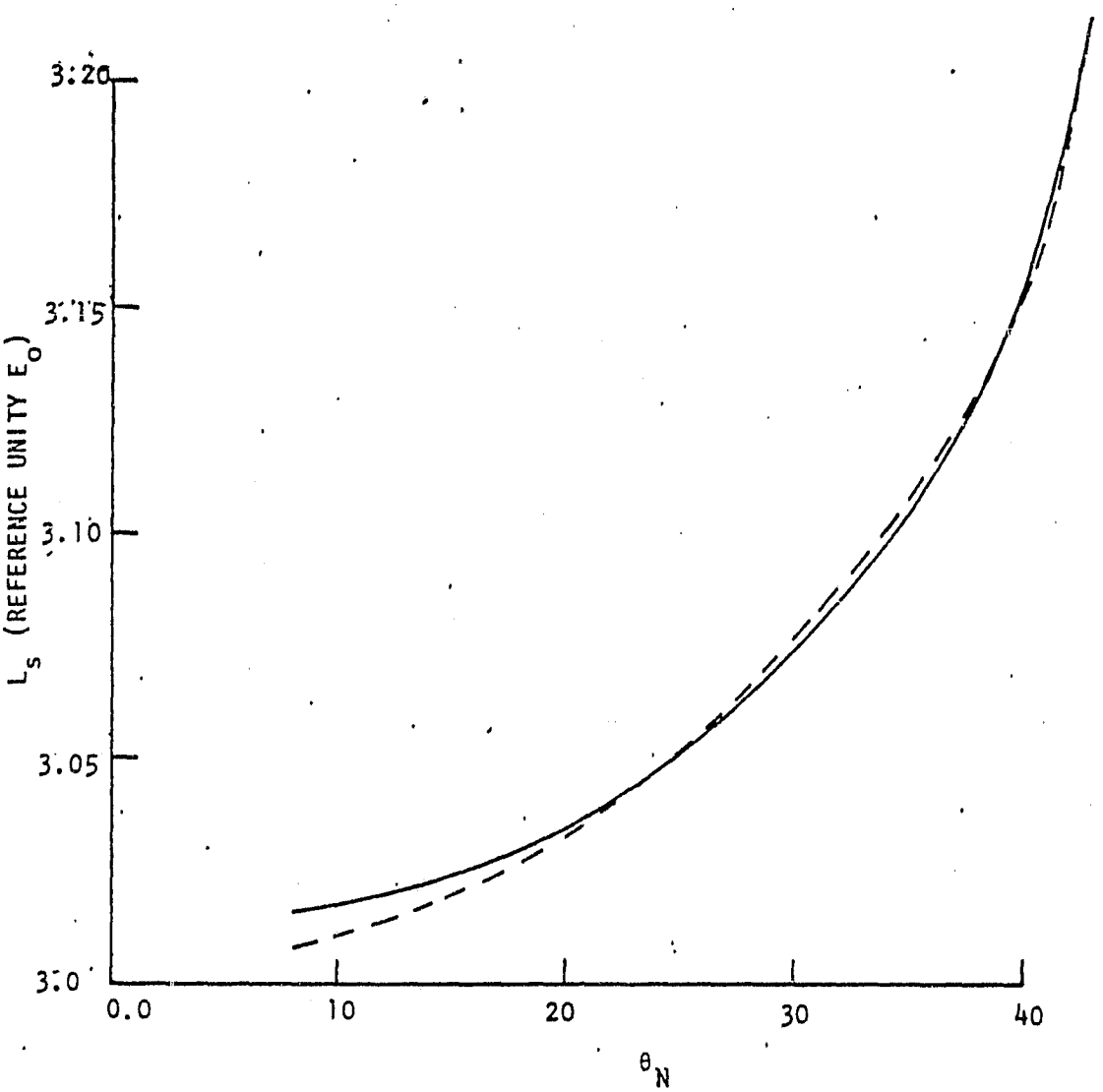

Fig. 22. Plot of SKYRAD predicted fit to input model calculation unknown. Solid line represents radiative transfer calculation model data versus nadir angle. Dashed line is curve predicted by SKYRAD.

FINAL RESULTANT PARAMETERS FOR MODEL DATA FIT

a_j	τ	ρ	E_D		L_p
Input	.2	.1	.1	.06	.06
Output	.158 ±.024	.104 ±.023	.124 ±.153	.061 ±.004	.059 ±.005
Model	0.185	0.1	0.095	0.062	0.060

Conclusion

The non-linear regression numerical technique described is a viable method for determining the path radiance and ground reflectance in remote-sensed scenes. The technique is not without inherent difficulty, most notably the problem of local minima. However, judicious application of the outlined analysis procedure and the careful evaluation of results yields parameters that are close to the correct values.

6.0 CONCLUSIONS & RECOMMENDATIONS

The following conclusions are drawn from this study:

1) The magnitude of the pointing angle from nadir should be restricted for atmospheric studies to no more than 50^{o}. The reason is that no gain in accuracy is achieved in determining atmospheric parameters using large pointing angles, while in practice, the larger ground projected IFOV and the greater path radiance crosstalk from surrounding ground areas may adversely affect the accuracy. In addition, engineering and multi-experiment requirements militate against the use of very large pointing angles.

2) An increase in the atmospheric extinction coefficient, τ, of 0.1 at 0.65 μm caused an average decrease in classification accuracy of 3%. Such a change in τ is large across a Landsat scene in a purely rural area. Thus atmospheric correction may not be an important task for a pointable imager for a rural scene. However, we should emphasize that we did not explore the case of low reflectances in bands 4 and 5 associated with very dense green vegetation. Also, this conclusion does not apply to the important case of classification in the transitional zone between urban and rural areas.

3) There is a significant asymmetry of classification accuracy between training and test data which indicates that, in general, it is preferable to train under hazy conditions and test under clear conditions

than vice versa. In addition, when training under clear and testing under hazy conditions, low reflectance features. Reversing the procedure caused high reflectance features to show a greater error than low reflectance features.

4) The two-wavelength approach to determining the extinction coefficient does not work under the conditions explored here.

5) The non-linear least squares regression method proved to be successful in determining the extinction coefficient, the ground reflectance and the path radiance. However, care had to be exercised in prudently choosing the starting input parameters and in analyzing the output data.

6) The analysis performed thus far does not indicate the need to extend the wavelength range beyond that required by other applications. Probably four bands in the range 0.45 - 0.75 μm should be sufficient to determine the spectral characteristics of the measured atmospheric parameters and to provide a check on the consistency of the results.

7) Although the relative radiometric accuracy question was not addressed in this study, there are indications that 8 bit quantization may be marginal for techniques involving subtraction of radiance values, e.g., the two wavelength method. If the option of 9 or 10 bit quantization exists, this question should be studied in detail. In any case future study should address the effect of quantization noise on classification accuracy.

8) Although the correction for atmospheric effects may not often be beneficial for improving classification accuracy across purely rural scenes the opportunity to obtain scene reflectance values should be of great importance both for feature identification purposes, and BRDF and polarization studies.

9) The results of this preliminary study are promising and indicate the feasibility of using a pointable imaging system (a) for the determination of the atmospheric parameters required to improve classification accuracies in urban--rural transitional zones and to apply in studies of BRDF and polarization effects and (b) for the determination of the spectral reflectances of ground features.

The following recommendations are made based on the results of this preliminary 6-month study. (Of the six months, approximately the first three were devoted to a literature study published in another report). Future work should consider:

1) Different combinations of solar zenith and azimuth angles.
2) The separation of very similar scene classes (e.g. vegetation types) and classes having low reflectance values.
3) The effect of detector noise on classification accuracy and reflectance estimation.
4) The effect of the number of quantization steps on classification accuracy and reflectance estimation.
5) The effect of an inhomogeneous atmosphere and a non-uniform ground scene.
6) The effect of changing probability thresholding on classification accuracy.
7) Typical natural variability differences between training and test areas.
8) The very important question of whether very rapid, atmospherically induced irradiance fluctuations render greater than 6 bit quantization meaningless.

7.0 REFERENCES

Bevington, P. R., Data Reduction and Error Analysis for the Physical Sciences, McGraw-Hill, Inc., New York, 1969

Elterman, L., "Vertical-Attenuation Model with Eight Surface Meteorological Range 2 to 13 Kilometers" AFCRL-70-0200, March 1970.

Flowers, E. E., McCormick, R. A., and Kurfis, R. R., "Atmospheric Turbidity Over the United States, 1961-65." J. of Applied Meteorology Vol. 8, p. 955, 1969.

Herman, B. M., Browning, S. R., The Effects of Aerosols on the Earth Atmosphere Albedo, J. Atmos. Sci. 32, (1430-1445) 1975.

Marquardt, D. W., An Algorithm for Least-Squares Estimation of Non-linear Parameters, J. Soc. Ind. Appl. Math, II, #2, (431-441) 1963.

Potter, J. and Shelton, M., "Effect of Atmospheric Haze and Sun Angle on Automatic Classification of ERTS-1 Data." Proc 9th International Symp. on Rem. Sens. of Environ, ERIM p. 865, 1974.

Slater, P.N., "Remote Sensing; Optics and Optical Systems." Addison-Wesley Advanced Book Program, March 1980.

Turner, R. E., "Signature Variations due to Atmospheric Effects" Proc 10th International Symp. on Rem. Sens. of Environ, ERIM, p. 671, 1975.

APPENDIX A

SKYRAD CODE LISTINGS AND SUBROUTINES

APPENDIX A

```
      PROGRAM SKYRAD (INPUT,OUTPUT,TAPE5,TAPE10,TAPE11)
C
C THIS ROUTINE UTILIZES THE NON-LINEAR REGRESSION SUBROUTINE CURFIT
C   TO FIT A SET OF DATA TO A SPECIFIED FUNCTION WHICH IS NON-LINEAR
C   IN ITS PARAMETERS.
C
C THE FUNCTION ANALYZED IS DEPENDENT ON FIVE PARAMETERS AND IS AN
C   EXPRESSION FOR THE TOTAL RADIANCE RECIEVED BY A POINTABLE REMOTE
C   SENSING SATELLITE-BASED RADIOMETER. (SEE SUBROUTINE FUNCT )
C
C THE SOURCE OF SUBROUTINES CURFIT, FDERIV, AND SCHISQ IS
C   BEVINGTON,P.R., DATA REDUCTION AND ERROR ANALYSIS FOR THE
C                   PHYSICAL SCIENCES, MCGRAW-HILL, 1969.
C
C DESCRIPTION OF PARAMETERS
C  X       : ARRAY OF INDEPENDENT VARIABLE (SECTHN)
C  Y       : ARRAY OF DEPENDENT VARIABLE (RECEIVED TOTAL RADIANCE)
C  SIGMAY  : ARRAY OF STANDARD DEVIATIONS FOR Y
C  A       : ARRAY OF FIT PARAMETERS FOR FUNCTION
C  DELTAA  : ARRAY OF INCREMENT VALUES FOR A
C  SIGMAA  : ARRAY OF STANDARD DEVIATIONS FOR A
C  YFIT    : ARRAY OF CALCULATED VALUES OF Y
C  NPTS    : NUMBER OF PAIRS OF DATA POINTS
C  NTERMS  : NUMBER OF FIT PARAMETERS
C  MODE    : DETERMINES METHOD OF STATISTICAL FIT (SEE CURFIT)
C  CHISQR  : REDUCED CHI SQUARE VALUE FOR FIT
C  E0      : EXTRATERRESTIAL SOLAR IRRADIANCE VALUE FOR SPECTRAL BAND
C
C INPUT (UNFORMATTED READS)
C     TAPE5  : CONTAINS X,Y,SIGMAY OUPUT OF SYNRAD OR REAL DATA
C     TAPE10 : NPTS,NTERMS,MODE,FLAMDA,A,DELTAA,E0
C     CARDS  : NFLG, IF NFLG = 1, PROGRAM READS TAPE10 INPUT FROM CARD
C
C OUTPUT (UNFORMATTED WRITES)
C     TAPE11 : NPTS,NTERMS,MODE,FLAMDA,A,DELTAA
C     PRINT  : RESULTS OF EACH ITERATION THROUGH CURFIT
C
C COMMENTS
C  1.) X,Y,SIGMAY,NPTS,NTERMS,MODE,FLAMDA,A,DELTAA,E0 MUST BE INPUT
C  2.) A,SIGMAA,YFIT,CHISQR IS OUTPUT
C  3.) FLAMDA IS SET TO 0.001 INITIALLY
C  4.) PROGRAM ITERATES THROUGH CURFIT  UNTIL TIME IS CONSUMED
C       OR DIFFERENCE OF CHISQR VALUES BETWEEN ITERATIONS IS < 0.001.
C       IF CHISQR CONDITION IS NOT MET FINAL FIT RESULTS ARE STORED IN
C       TAPE11 TO BE USED FOR NEXT RUN OF SKYRAD.
C  5.) PROPER COMMON BLOCK SPECIFICATION IS NECESSARY
C  6.) BEVINGTON SUBROUTINES CURFIT, FDERIV, SCHISQ ARE NEEDED
C
C THE ROUTINE WAS CODED IN FORTRAN FOR A CDC CYBER 175,
C   BY S.J. MARTINEK, OPTICAL SCIENCES CENTER, OCTOBER 1979
C
      COMMON /ARRAY1/ X(16), A(5), DELTAA(5), SIGMAA(5)
      COMMON /ARRAY2/ Y(16), YFIT(16), SIGMAY(16)
      COMMON / / CHISQR, FLAMDA, E0 /NUM/ NPTS, NTERMS, MODE
      DATA SIGMAA /5*0.0/
C
C INPUT DATA
```

```
      PROGRAM SKYPAD     74/74   OPT=2

                  READ(5) X,Y,SIGMAY
                  READ*, NFLG
      60          IF(NFLG) 2,2,3
                2 READ(10) NPTS,NTERMS,MODE,FLAMDA,A,DELTAA,E0
                  GO TO 4
                3 READ*, NPTS,NTERMS,MODE,FLAMDA,A,DELTAA,E0
                4 CONTINUE
      65        C
                C CALL CURFIT, PRINT RESULTS, AND ITERATE
                  K = 0    3    CHISQR = 0.
                  PRINT 50    3    PRINT 55, K,CHISQR,FLAMDA
                  DO 5 I=1,NTERMS
      70        5   PRINT 60, I,A(I),SIGMAA(I),DELTAA(I)
                  CHITEST = 1.0
                  DO 15 K=1,35
                    IF(MOD(K,4).EQ.0) PRINT 49
                    CALL CURFIT
      75            PRINT 56, K,CHISQR,FLAMDA
                    DO 10 I=1,NTERMS
                10    PRINT 61, I,A(I),SIGMAA(I)
                    IF (CHISQR.EQ.0.0) GO TO 20
                    C = ABS(CHISQR-CHITEST)/CHITEST
      80            IF(C.LT.0.010) GO TO 20
                    CHITEST = CHISQR
                15 CONTINUE
                20 CONTINUE
                   IF(K.EQ.36) K = K-1
      85        C
                C OUTPUT RESULTS
                   WRITE(11) NPTS,NTERMS,MODE,FLAMDA,A,DELTAA,E0
                   PRINT 65, K
                   DO 25 I=1,NPTS
      90             AE = Y(I)-YFIT(I)
                     PE = AE/Y(I)*100.
                     PRINT 70, I,X(I),Y(I),YFIT(I),AE,PE
                25 CONTINUE
      95        C
                C COMPUTE & PRINT PATH RADIANCE FOR SEC(THN) = 1.
                   PRAD = A(4) + A(5)*EXP(-A(1))
                   PRINT 75, PRAD
                C
                C FORMAT STATEMENTS
     100           49 FORMAT(1H1///)
                   50 FORMAT(1H1//30X,"CURFIT ANALYSIS OF RADIANCE EXPRESSION"//13X
                     2 ,"A1 = TAU ; A2 = RHO ; A3 = EDIFF ; A4,A5 = EXPANSION CONSTANTS
                     3 " FOR PATH RADIANCE"/)
                   55 FORMAT(1H0/20X,"FIT ITERATION",I3,5X,"CHISQR =",F8.3,5X,
     105             2 "FLAMDA =",1PE8.1//56X,"A",13X,"DELA"/)
                   56 FORMAT(1H0/20X,"FIT ITERATION",I3,5X,"CHISQR =",F8.3,5X,
                     2 "FLAMDA =",1PE8.1//51X,"A")
                   60 FORMAT(1H ,30X,I5,3X,1PE11.4," +/-",E11.4,4X,"(",E11.4,")")
                   61 FORMAT(1H ,30X,I5,3X,1PE11.4," +/-",E11.4)
     110           65 FORMAT(1H1///20X,"ERRORS IN RESULTS FOR ITERATION",I3//32X,
                     2 "X",11X,"Y",8X,"YFIT",5X,"ABS ERR",6X,"PERCNT"/)
                   70 FORMAT(1H ,20X,I3,F9.2,4(1PE12.3))
                   75 FORMAT(1H0/15X,"THE UPWELLING PATH RADIANCE IS",1PE12.3,
                     2 " FOR A NADIR ANGLE OF ZERO")
```

SUBROUTINE CURFIT 74/74 OPT=2

```
      SUBROUTINE CURFIT
C
C PURPOSE : MAKE A LEAST-SQUARES FIT TO A NON-LINEAR FUNCTION
C   VIA THE MARQUUARDT APPROACH (SEE BEVINGTON P,232)
C
C PARAMETER DESCRIPTION
C  X       : ARRAY OF DATA POINTS FOR THE INDEPENDENT VARIABLE
C  Y       : ARRAY OF DATA POINTS FOR THE DEPENDENT VARIABLE
C  SIGMAY  : ARRAY OF STANDARD DEVIATIONS FOR DEPENDENT VARAIBLE
C  NPTS    : NUMBER OF PAIRS OF DATA POINTS
C  NTERMS  : NUMBER OF FIT PARAMETERS
C  MODE    : DETERMINES METHOD OF WEIGHTING LEAST-SQUARES FIT
C            +1 (INSTRUMENTAL) WEIGHT(I) = 1./SIGMAY(I)**2
C             0 (NO WEIGHTING) WEIGHT(I) = 1.
C            -1 (STATISTICAL) WEIGHT(I) = 1./Y(I)
C  A       : ARRAY OF FIT PARAMETERS
C  DELTAA  : ARRAY OF INCREMENTS FOR PARAMETERS A
C  SIGMAA  : ARRAY OF STANDARD DEVIATIONS FOR PARAMETERS A
C  FLAMDA  : PROPORTION OF GRADIENT SEARCH INCLUDED
C  YFIT    : ARRAY OF CALCULATED VALUES OF Y
C  CHISQR  : REDUCED CHI SQUARE FOR FIT
C
C SUBROUTINES AND FUNCTION SUBROUTINES REQUIRED
C   FUNCT   : EVALUATES THE FITTING FUNCTION
C   SCHISQ  : EVALUATES REDUCED CHISQR FOR FIT TO DATA
C   FDERIV  : EVALUATES THE DERIVATIVE OF THE FITTING FUNCTION
C             FOR ALL X VALUES FOR EACH PARAMETER
C   MXINV   : INVERTS THE MATRIX
C
C COMMENTS
C   COMMON BLOCK SPECIFICATIONS ARE CRUCIAL FOR PARAMETERS
C   DIMENSION STATEMNT VALID FOR NTERMS UPTO 10, NPTS = 16
C   SET FLAMDA = 0.001 AT BEGINNING OF SEARCH
C NOTE : BEVINGTON ROUTINE HAS BEEN ALTERED TO ONLY LOOK FOR POSITIVE P
C
      COMMON /ARRAY1/ X(16), A(5), DELTAA(5), SIGMAA(5)
      COMMON /ARRAY2/ Y(16), YFIT(16), SIGMAY(16)
      COMMON / / CHISQR, FLAMDA, E0 /NUM/ NPTS, NTERMS, MODE
      COMMON /ARRAY3/ DERIV(10,16), ARRAY(10,10) /1/ NORDER
      DIMENSION WEIGHT(100), ALPHA(10,10), BETA(10), B(10), ADUM(10)
C
      NORDER = NTERMS
      NFREE = NPTS-NTERMS
      IF(NFREE) 13,13,20
   13 CHISQR = 0.
      GO TO 110
C
C EVALUATE WEIGHTS
   20 DO 30 I=1,NPTS
         IF(MODE) 22,27,29
   22    IF(Y(I)) 25,27,23
   23    WEIGHT(I) = 1./Y(I)
         GO TO 30
   25    WEIGHT(I) = 1./(-Y(I))
         GO TO 30
   27    WEIGHT(I) = 1.
```

```
SUBROUTINE CURFIT     74/74   OPT=2

                    GO TO 30
                 29   WEIGHT(I) = 1./SIGMAY(I)**2
                 30 CONTINUE
               C
               C EVALUATE ALPHA AND BETA MATRICES
                    DO 34 J=1,NTERMS
                      BETA(J) = 0.
                      DO 34 K=1,J
                 34     ALPHA(J,K) = 0.
                    CALL FDERIV
                    CALL FUNCT
                    DO 50 I=1,NPTS
                      DO 46 J=1,NTERMS
                        BETA(J) = BETA(J) + WEIGHT(I)*(Y(I)-YFIT(I))*DERIV(J,I)
                        DO 46 K=1,J
                 46     ALPHA(J,K) = ALPHA(J,K) + WEIGHT(I)*DERIV(J,I)*DERIV(K,I)
                 50 CONTINUE
                    DO 53 J=1,NTERMS
                      DO 53 K=1,J
                 53     ALPHA(K,J) = ALPHA(J,K)
               C
               C EVALUATE CHI SQUARE AT STARTING POINT
                    CALL SCHISQ
                    CHISQ1 = CHISQR
               C
               C INVERT MODIFIED CURVATURE MATRIX TO FIND NEW PARAMETERS
                    KK = 0    $   NN = 0
                 71 KK = KK+1
                    DO 74 J=1,NTERMS
                    DO 73 K=1,NTERMS
                 73   ARRAY(J,K) = ALPHA(J,K)/SQRT(ALPHA(J,J)*ALPHA(K,K))
                 74   ARRAY(J,J) = 1.+FLAMDA
                    CALL MXINV
                    DO 84 J=1,NTERMS
                    B(J) = ADUM(J) = A(J)
                    DO 84 K=1,NTERMS
                 84   B(J) = B(J)+BETA(K)*ARRAY(J,K)/SQRT(ALPHA(J,J)*ALPHA(K,K))
                    DO 85 J=1,NTERMS
                 85   A(J) = B(J)
               C
               C IF CHI SQUARE INCREASED, INCREASE FLAMDA AND TRY AGAIN
                    CALL FUNCT
                    CALL SCHISQ
                    PRINT 150, KK,FLAMDA,CHISQ1,CHISQR
                150 FORMAT(1H0,17X,"LAMDA ITERATION",I3,3X,"FLAMDA =",1PE8.1,3X,
                   2 "CHISQ1 =",0PF8.3,3X,"CHISQR =",F8.3)
               C
               C CHECK IF PARAMETERS HAVE GONE NEGATIVE AND TRY TO FORCE POSITIVE
                    NN = NN+1
                    XX = AMIN1(A(1),A(2),A(3),A(4),A(5))
                    IF(XX) 86,86,90
                 86 PRINT 151, NN
                151 FORMAT(1H0,23X,"NEGATIVE PARAMETER ITERATION",I3)
                    IF(NN.LT.7) GO TO 95
                    PRINT 152
                152 FORMAT(1H0,7X,"FIT TERMINATION : CANNOT AVOID OPTIMIZING A"
                   2 " NEGATIVE PARAMETER VALUE")
```

```
      SUBROUTINE CURFIT      74/74   OPT=2

115                CHISQR = 0.0
                   GO TO 101
                90 IF(CHISQ1-CHISQR) 95,101,101
                95 FLAMDA = 10.*FLAMDA
                   DO 96 J=1,NTERMS
125             96   A(J) = ADUM(J)
                   GO TO 71
                C
                C EVALUATE PARAMETERS AND UNCERTAINTIES
                101  DO 103 J=1,NTERMS
125             103  SIGMAA(J) = SQRT(ARRAY(J,J)/ALPHA(J,J))
                     FLAMDA = FLAMDA/10.
                110  RETURN
                     END
```

```
SUBROUTINE FUNCT      74/74   OPT=2

1
                      SUBROUTINE FUNCT
                C
                C THIS ROUTINE COMPUTES YFIT, FOR ALL X, FOR A GIVEN CALL
5               C
                C  YFIT(I) = A4 + ((E0*EXP(-A1*SECTHZ) + A3)*A2/PI - A5)*EXP(-A1*X(I))
                C
                C  CONSTRAINTS :
                C  1.) A SOLAR ZENITH ANGLE OF 45DEG IS ASSUMED
10              C  2.) E0 = E0*COS(THZ)
                C
                       COMMON /ARRAY1/ X(16), A(5), DELTAA(5), SIGMAA(5)
                       COMMON /ARRAY2/ Y(16), YFIT(16), SIGMAY(16)
                       COMMON / / CHISQR, FLAMDA, E0 /NUM/ NPTS, NTERMS, MODE
15              C
                       PI = ACOS(-1.)    $   RPD = PI/180.   $   THZ = 45.
                       A1 = A(1)   $   A2 = A(2)   $   A3 = A(3)   $   A4 = A(4)   $   A5 = A(5)
                C
                C COMPUTE TERMS OF EXPRESSION
20                     ET = EXP(-A1)
                       RMZ = 1./COS(THZ*RPD)
                       P1 = E0*ET**RMZ/RMZ
                       P2 = (P1+A3)*A2/PI - A5
                C
25              C FILL YFIT ARRAY
                       DO 5 I=1,NPTS
                         YFIT(I) = A4 + P2*ET**X(I)
                     5 CONTINUE
                       RETURN
30                     END
```

SUBROUTINE FDERIV 74/74 OPT=2

```
      SUBROUTINE FDERIV
C PURPOSE : EVALUATE DERIVATIVES OF FUNCTION FOR LEAST-SQRAURES SEARCH
C   AT EACH POINT X WRT EACH FIT PARAMETER
C
C        FOR ARBITRARY FUNCTION GIVEN BY FUNCT
C
C SEE BEVINGTON, P242
C
C DESCRIPTION OF PARAMETERS
C  X       : ARRAY OF DATA POINTS FOR INDEPENDENT VARIABLE
C  I       : INDEX OF DATA POINTS
C  A       : ARRAY OF PARAMETERS
C  DELTAA  : ARRAY OF PARAMETER INCREMENTS
C  NTERMS  : NUMBER OF PARAMETERS
C  DERIV   : DERIVATIVES OF FUNCTION
C
      COMMON /ARRAY1/ X(16), A(5), DELTAA(5), SIGMAA(5)
      COMMON /ARRAY2/ Y(16), YFIT(16), SIGMAY(16)
      COMMON / / CHISQR, FLAMDA, E0 /NUM/ NPTS, NTERMS, MODE
      COMMON /ARRAY3/ DERIV(10,16), ARRAY(10,10) /1/ NORDER
      DIMENSION Y1(32)
C
      DO 15 J=1,NTERMS
        AJ = A(J)    S    DEL = DELTAA(J)
        A(J) = AJ + DEL
        CALL FUNCT
        DO 5 I=1,NPTS
    5     Y1(I) = YFIT(I)
        A(J) = AJ-DEL
        CALL FUNCT
        DO 10 I=1,NPTS
   10     DERIV(J,I) = (Y1(I)-YFIT(I))/(2.*DEL)
        A(J) = AJ
   15 CONTINUE
      RETURN
      END
```

```
SUBROUTINE SCHISQ     74/74   OPT=2

                      SUBROUTINE SCHISQ
                C     EVALUATES THE REDUCED CHI SQUARE FOR FIT TO DATA
                C       CHISQR = SUM ((Y-YFIT)**2/SIGMA**2)/NFREE
                C     SEE BEVINGTON, P193
                C     USAGE  :  PROPER COMMON BLOCK SPECIFICATION
                C     DESCRIPTION OF PARAMETERS :
                C       Y       - ARRAY OF DATA POINTS
                C       SIGMAY  - ARRAY OF STANDARD DEVIATIONS FOR DATA POINTS
                C       NPTS    - NUMBER OF DATA POINTS
                C       NFREE   - NUMBER OF DEGREES OF FREEDOM
                C       MODE    - DETERMINES METHOD OF WEIGHTING LEAST-SQUARES FIT
                C                 +1 (INSTRUMENTAL) WEIGHT(I) = 1./SIGMAY(I)**2
                C                  0 (NO WEIGHTING) WEIGHT(I) = 1.
                C                 -1 (STATISTICAL) WEIGHT(I) = 1./Y(I)
                C       YFIT    - ARRAY OF CALCULATED VALUES OF Y
                C       CHISQR  - REDUCED CHI SQUARE FOR FIT
                C
                        COMMON /ARRAY1/ X(16), A(5), DELTAA(5), SIGMAA(5)
                        COMMON /ARRAY2/ Y(16), YFIT(16), SIGMAY(16)
                        COMMON / / CHISQR, FLAMDA, E0 /NUM/ NPTS, NTERMS, MODE
                C
                        CHISQ = 0.
                        NFREE = NPTS-NTERMS
                        IF(NFREE) 13,13,20
                     13 CHISQR = 0.
                        GO TO 40
                C
                C     ACCUMULATE CHI SQUARE
                C
                     20 DO 30 I=1,NPTS
                        IF(MODE) 22,27,29
                     22 IF(Y(I)) 25,27,23
                     23 WEIGHT = 1./Y(I)
                        GO TO 30
                     25 WEIGHT = 1/(-Y(I))
                        GO TO 30
                     27 WEIGHT = 1.
                        GO TO 30
                     29 WEIGHT = 1./SIGMAY(I)**2
                     30 CHISQ = CHISQ + WEIGHT*(Y(I)-YFIT(I))**2
                C
                C     DIVIDE BY NUMBER OF DEGREES OF FREEDOM
                C
                        FREE = NFREE
                        CHISQR = CHISQ/FREE
                     40 RETURN
                        END
```

SUBROUTINE MXINV 74/74 OPT=2

```
      SUBROUTINE MXINV
C
C THE OBJECTIVE OF THIS ROUTINE IS TO COMPUTE THE INVERSE OF MARRIX
C   ARRAY.  THE METHOD USED IS GAUSS-JORDAN, NO ROW SUBSTITUTIONS.
C   THE MATRIX ARRAY IS ASSUMED TO BE NON-SINGULAR AND THE DIAGONAL
C   ELEMENTS ARE USED AS PIVOTS.
C   NOTE !!!  THE ORIGINAL MATRIX ARRAY IS DESTROYED.  THE INVERSE IS
C   RETURNED IN MATRIX ARRAY
C
      COMMON /ARRAY3/ DERIV(10,16), ARRAY(10,10) /1/ NORDER
      REAL INV(10,10)
C
C PUT IDENTITY MATRIX IN INVERSE MATRIX ARRAY
      N = NORDER
      DO 20 I=1,N
        DO 25 J=1,N
          INV(I,J) = 0.
   25   CONTINUE
          INV(I,I) = 1.
   20 CONTINUE
C
C FIND INVERSE USING GAUSS-JORDAN METHOD
      DO 50 I=1,N
C
C SELECT PIVOT ELEMENT
      ALPHA = ARRAY(I,I)
C
C DIVIDE PIVOT ROW BY PIVOT ELEMENT
      DO 30 J=1,N
        ARRAY(I,J) = ARRAY(I,J)/ALPHA
        INV(I,J) = INV(I,J)/ALPHA
   30 CONTINUE
C
C FOR OTHER ROWS, SUBTRACT MULTIPLIER TIMES PIVOT ROW FROM ROW
      DO 40 K=1,N
        IF(K.EQ.I)  GO TO 40
        BETA = ARRAY(K,I)
        DO 35 L=1,N
          ARRAY(K,L) = ARRAY(K,L)-BETA*ARRAY(I,L)
          INV(K,L) = INV(K,L)-BETA*INV(I,L)
   35     CONTINUE
   40   CONTINUE
   50 CONTINUE
C
C FILL ARRAY WITH INVERSE VALUES
      DO 60 J=1,N
        DO 60 I=1,N
          ARRAY(I,J) = INV(I,J)
   60 CONTINUE
      RETURN
      END
```

APPENDIX B

SAMPLE SKYRAD OUTPUT

APPENDIX B

SAMPLE SKYRAD OUTPUT

```
                    CURFIT ANALYSIS OF RADIANCE EXPRESSION

A1 = TAU ; A2 = RHO ; A3 = EDIFF ; A4,A5 = EXPANSION CONSTANTS FOR PATH RADIANCE


  FIT ITERATION  0     CHISQR =    0.000     FLAMDA = 1.0E-03

                                      A              DELA

                  1    7.5000E-02 +/- 0.          ( 1.0000E-02)
                  2    2.5000E-01 +/- 0.          ( 1.0000E-02)
                  3    5.0000E-02 +/- 0.          ( 1.0000E-02)
                  4    7.5000E-02 +/- 0.          ( 1.0000E-02)
                  5    7.5000E-02 +/- 0.          ( 1.0000E-02)

LAMDA ITERATION  1   FLAMDA = 1.0E-03   CHISQ1 =2038.036   CHISQR =   1.261


  FIT ITERATION  1     CHISQR =   1.261     FLAMDA = 1.0E-04

                                      A
                  1    1.1223E-01 +/- 1.0793E-02
                  2    2.5705E-01 +/- 4.2369E-03
                  3    6.9344E-02 +/- 1.1625E-02
                  4    7.6956E-02 +/- 8.0884E-04
                  5    7.3461E-02 +/- 9.2510E-04

LAMDA ITERATION  1   FLAMDA = 1.0E-04   CHISQ1 =   1.261   CHISQR =    .764


  FIT ITERATION  2     CHISQR =    .764     FLAMDA = 1.0E-05

                                      A
                  1    1.4099E-01 +/- 2.0926E-02
                  2    2.5813E-01 +/- 1.4282E-02
                  3    7.2170E-02 +/- 3.7374E-02
                  4    7.7635E-02 +/- 2.3845E-03
                  5    7.3229E-02 +/- 3.0580E-03

LAMDA ITERATION  1   FLAMDA = 1.0E-05   CHISQ1 =    .764   CHISQR =    .444


  FIT ITERATION  3     CHISQR =    .444     FLAMDA = 1.0E-06

                                      A
                  1    1.3761E-01 +/- 6.3818E-02
                  2    2.5694E-01 +/- 4.8223E-02
                  3    6.9173E-02 +/- 1.2170E-01
                  4    7.8078E-02 +/- 7.4089E-03
                  5    7.3476E-02 +/- 9.9998E-03
```

```
LAMDA ITERATION  1   FLAMDA = 1.0E-06   CHISQ1 =    .444   CHISQR =   1.836
LAMDA ITERATION  2   FLAMDA = 1.0E-05   CHISQ1 =    .444   CHISQR =    .444

 FIT ITERATION  4     CHISQR =    .444     FLAMDA = 1.0E-06

                              A
          1    1.3420E-01 +/- 6.1080E-02
          2    2.5588E-01 +/- 4.8011E-02
          3    6.6468E-02 +/- 1.2168E-01
          4    7.8517E-02 +/- 7.4740E-03
          5    7.3697E-02 +/- 9.9523E-03
```

ERRORS IN RESULTS FOR ITERATION 4

	X	Y	YFIT	ABS ERR	PERCNT
1	1.00	6.063E-02	6.046E-02	1.618E-04	2.669E-01
2	1.00	6.056E-02	6.047E-02	9.088E-05	1.501E-01
3	1.01	6.052E-02	6.049E-02	3.300E-05	5.453E-02
4	1.02	6.051E-02	6.052E-02	-1.225E-05	-2.025E-02
5	1.04	6.052E-02	6.056E-02	-4.058E-05	-6.705E-02
6	1.06	6.056E-02	6.062E-02	-5.803E-05	-9.582E-02
7	1.09	6.063E-02	6.069E-02	-6.604E-05	-1.089E-01
8	1.13	6.072E-02	6.078E-02	-6.156E-05	-1.014E-01
9	1.15	6.078E-02	6.083E-02	-5.416E-05	-8.910E-02
10	1.18	6.083E-02	6.089E-02	-6.215E-05	-1.022E-01
11	1.21	6.091E-02	6.096E-02	-4.599E-05	-7.551E-02
12	1.24	6.100E-02	6.103E-02	-2.620E-05	-4.295E-02
13	1.27	6.110E-02	6.110E-02	-3.372E-06	-5.518E-03
14	1.31	6.120E-02	6.119E-02	1.180E-05	1.927E-02
15	1.35	6.133E-02	6.128E-02	4.850E-05	7.908E-02
16	1.39	6.149E-02	6.138E-02	1.058E-04	1.721E-01

THE UPWELLING PATH RADIANCE IS 1.408E-02 FOR A NADIR ANGLE OF ZERO

APPENDIX C

SAMPLE OUTPUT OF RADIATIVE TRANSFER COMPUTATION

APPENDIX C

SAMPLE OUTPUT OF RADIATIVE TRANSFER COMPUTATION

ATMOSPHERE = U25

WAVELENGTH = .50 MICRONS

TAU MIE = .498

TAU RAY = .145

TAU TOTAL = .643

ZENITH ANGLE OF SUN = 45.0 DEGREES

NADIR ANGLE (DEG)	TRANSMISSION EXP(-TAU X SEC(N))
5.0	.5244
15.0	.5139
25.0	.4916
35.0	.4561
45.0	.4028
55.0	.3259
65.0	.2184

NADIR ANGLE (DEG)	AZIMUTH (DEG)	GROUND ALBEDO 0.0 I	0.1 I	0.1 I-I'	.25 I	.25 I-I'	.5 I	.5 I-I'	.75 I	.75 I-I'
5.	0.	.2315E-01	.3970E-01	.2987E-01	.6597E-01	.4055E-01	.1141E+00	.6010E-01	.1684E+00	.8215E-01
5.	30.	.2323E-01	.3978E-01	.2995E-01	.6605E-01	.4063E-01	.1142E+00	.6018E-01	.1685E+00	.8223E-01
5.	60.	.2343E-01	.3997E-01	.3015E-01	.6625E-01	.4083E-01	.1144E+00	.6038E-01	.1687E+00	.8243E-01
5.	90.	.2379E-01	.4034E-01	.3052E-01	.6661E-01	.4120E-01	.1147E+00	.6075E-01	.1690E+00	.8280E-01
5.	120.	.2417E-01	.4071E-01	.3089E-01	.6699E-01	.4157E-01	.1151E+00	.6112E-01	.1694E+00	.8317E-01
5.	150.	.2450E-01	.4105E-01	.3123E-01	.6732E-01	.4191E-01	.1154E+00	.6145E-01	.1697E+00	.8350E-01
5.	180.	.2464E-01	.4119E-01	.3137E-01	.6746E-01	.4205E-01	.1156E+00	.6160E-01	.1699E+00	.8365E-01
15.	0.	.2297E-01	.3928E-01	.2966E-01	.6518E-01	.4027E-01	.1126E+00	.5969E-01	.1661E+00	.8160E-01
15.	30.	.2306E-01	.3937E-01	.2974E-01	.6526E-01	.4035E-01	.1127E+00	.5978E-01	.1662E+00	.8169E-01
15.	60.	.2344E-01	.3975E-01	.3012E-01	.6564E-01	.4074E-01	.1131E+00	.6016E-01	.1666E+00	.8207E-01
15.	90.	.2424E-01	.4055E-01	.3093E-01	.6645E-01	.4154E-01	.1139E+00	.6096E-01	.1674E+00	.8287E-01
15.	120.	.2554E-01	.4184E-01	.3222E-01	.6774E-01	.4283E-01	.1152E+00	.6226E-01	.1687E+00	.8417E-01
15.	150.	.2693E-01	.4324E-01	.3361E-01	.6913E-01	.4423E-01	.1165E+00	.6365E-01	.1701E+00	.8556E-01
15.	180.	.2771E-01	.4401E-01	.3439E-01	.6991E-01	.4500E-01	.1173E+00	.6443E-01	.1708E+00	.8634E-01
25.	0.	.2439E-01	.4048E-01	.3127E-01	.6602E-01	.4218E-01	.1128E+00	.6216E-01	.1656E+00	.8469E-01
25.	30.	.2439E-01	.4048E-01	.3126E-01	.6602E-01	.4218E-01	.1128E+00	.6216E-01	.1656E+00	.8469E-01
25.	60.	.2452E-01	.4061E-01	.3140E-01	.6616E-01	.4231E-01	.1129E+00	.6229E-01	.1657E+00	.8483E-01
25.	90.	.2546E-01	.4155E-01	.3234E-01	.6709E-01	.4325E-01	.1139E+00	.6323E-01	.1666E+00	.8576E-01
25.	120.	.2752E-01	.4361E-01	.3440E-01	.6915E-01	.4531E-01	.1159E+00	.6529E-01	.1687E+00	.8782E-01
25.	150.	.3086E-01	.4695E-01	.3773E-01	.7249E-01	.4865E-01	.1193E+00	.6863E-01	.1720E+00	.9116E-01
25.	180.	.3350E-01	.4959E-01	.4037E-01	.7513E-01	.5129E-01	.1219E+00	.7127E-01	.1747E+00	.9380E-01
35.	0.	.2781E-01	.4360E-01	.3505E-01	.6866E-01	.4655E-01	.1145E+00	.6759E-01	.1663E+00	.9132E-01
35.	30.	.2742E-01	.4320E-01	.3466E-01	.6826E-01	.4615E-01	.1141E+00	.6719E-01	.1659E+00	.9092E-01
35.	60.	.2700E-01	.4278E-01	.3424E-01	.6784E-01	.4574E-01	.1137E+00	.6678E-01	.1655E+00	.9050E-01
35.	90.	.2765E-01	.4343E-01	.3489E-01	.6849E-01	.4638E-01	.1144E+00	.6742E-01	.1662E+00	.9115E-01
35.	120.	.3030E-01	.4609E-01	.3754E-01	.7114E-01	.4904E-01	.1170E+00	.7008E-01	.1688E+00	.9381E-01
35.	150.	.3633E-01	.5211E-01	.4357E-01	.7717E-01	.5506E-01	.1231E+00	.7610E-01	.1748E+00	.9983E-01
35.	180.	.4237E-01	.5815E-01	.4961E-01	.8321E-01	.6111E-01	.1291E+00	.8215E-01	.1809E+00	.1059E+00
45.	0.	.3513E-01	.5041E-01	.4286E-01	.7465E-01	.5513E-01	.1190E+00	.7759E-01	.1691E+00	.1029E+00
45.	30.	.3372E-01	.4899E-01	.4145E-01	.7324E-01	.5372E-01	.1176E+00	.7617E-01	.1677E+00	.1015E+00
45.	60.	.3139E-01	.4666E-01	.3912E-01	.7091E-01	.5139E-01	.1153E+00	.7384E-01	.1654E+00	.9916E-01
45.	90.	.3131E-01	.4658E-01	.3903E-01	.7083E-01	.5131E-01	.1152E+00	.7376E-01	.1653E+00	.9908E-01
45.	120.	.3426E-01	.4954E-01	.4199E-01	.7379E-01	.5426E-01	.1182E+00	.7672E-01	.1683E+00	.1020E+00
45.	150.	.4168E-01	.5696E-01	.4941E-01	.8121E-01	.6166E-01	.1256E+00	.8414E-01	.1757E+00	.1095E+00
45.	180.	.5138E-01	.6666E-01	.5911E-01	.9090E-01	.7138E-01	.1353E+00	.9384E-01	.1854E+00	.1192E+00
55.	0.	.4710E-01	.6153E-01	.5543E-01	.8445E-01	.6866E-01	.1264E+00	.9286E-01	.1737E+00	.1201E+00
55.	30.	.4431E-01	.5874E-01	.5264E-01	.8166E-01	.6587E-01	.1236E+00	.9007E-01	.1709E+00	.1174E+00
55.	60.	.3886E-01	.5330E-01	.4719E-01	.7622E-01	.6042E-01	.1182E+00	.8462E-01	.1655E+00	.1119E+00
55.	90.	.3721E-01	.5165E-01	.4554E-01	.7457E-01	.5877E-01	.1165E+00	.8298E-01	.1639E+00	.1103E+00
55.	120.	.3989E-01	.5432E-01	.4822E-01	.7724E-01	.6145E-01	.1192E+00	.8565E-01	.1665E+00	.1129E+00
55.	150.	.4740E-01	.5184E-01	.5573E-01	.8476E-01	.6896E-01	.1267E+00	.9316E-01	.1740E+00	.1204E+00
55.	180.	.5753E-01	.7196E-01	.6586E-01	.9489E-01	.7909E-01	.1368E+00	.1033E+00	.1842E+00	.1306E+00
65.	0.	.6792E-01	.8101E-01	.7692E-01	.1018E+00	.9119E-01	.1398E+00	.1173E+00	.1826E+00	.1467E+00
65.	30.	.6240E-01	.7548E-01	.7139E-01	.9625E-01	.8567E-01	.1343E+00	.1118E+00	.1771E+00	.1412E+00
65.	60.	.5197E-01	.6505E-01	.6096E-01	.8582E-01	.7524E-01	.1238E+00	.1014E+00	.1667E+00	.1308E+00
65.	90.	.4653E-01	.5961E-01	.5552E-01	.8038E-01	.6980E-01	.1184E+00	.9591E-01	.1613E+00	.1253E+00
65.	120.	.4861E-01	.6169E-01	.5760E-01	.8246E-01	.7188E-01	.1205E+00	.9799E-01	.1633E+00	.1274E+00
65.	150.	.5201E-01	.6509E-01	.6100E-01	.8586E-01	.7527E-01	.1239E+00	.1014E+00	.1667E+00	.1308E+00
65.	180.	.6344E-01	.7652E-01	.7243E-01	.9729E-01	.8671E-01	.1353E+00	.1128E+00	.1782E+00	.1423E+00